

Fission and fusion of heavy nuclei induced by the passage of a radiation-mediated shock in BNS mergers

Alon Granot^{*}, Amir Levinson, Ehud Nakar

School of Physics and Astronomy, Tel Aviv University, Tel Aviv 69978, Israel

May 2024

ABSTRACT

We compute the structure of a Newtonian, multi-ion radiation-mediated shock (RMS) for different compositions anticipated in various stellar explosions. We use a multifluid RMS model that incorporates electrostatic coupling between the different plasma constituents as well as Coulomb friction in a self-consistent manner, and approximates the effect of pair creation and the presence of free neutrons in the shock upstream on the shock structure. We find that under certain conditions a significant velocity separation is developed between different ions in the shock downstream and demonstrate that in fast enough shocks ion-ion collisions may trigger fusion and fission events at a relatively high rate. Our analysis ignores anomalous coupling through plasma microturbulence, that might reduce the velocity spread downstream below the activation energy for nuclear reactions. A rough estimate of the scale separation in RMS suggests that for shocks propagating in BNS merger ejecta the anomalous coupling length may exceed the radiation length, allowing a considerable composition change behind the shock via inelastic collisions of α particles with heavy elements at shock velocities $\beta_u \gtrsim 0.25$. A sufficient abundance of free neutrons in the shock upstream, as expected during the first second after the merger, is also expected to alter the ejecta composition through neutron capture downstream. The resultant change in the composition profile may affect the properties of the early kilonova emission. The generation of microturbulence due to velocity separation can also give rise to particle acceleration that might alter the breakout signal in supernovae and other systems.

Key words: Transients – Shock Waves – Plasmas – Nucleosynthesis

1 INTRODUCTION

Radiation mediated shocks (RMS) are inherent in essentially all (strong) stellar explosions (e.g., various types of supernovae, low luminosity GRBs, regular GRBs, binary neutron star mergers and tidal disruption events). They dictate the properties of the early electromagnetic emission released in the explosion during the breakout of the shock from the opaque envelope enshrouding the source, the detection of which is a primary focus of current and upcoming transient surveys (for recent reviews see Waxman & Katz 2017; Levinson & Nakar 2020). The RMS structure and dynamics depend on the progenitor type, the explosion energy and the explosion geometry. In particular, the shock velocity at breakout can range from sub-relativistic to mildly relativistic, and in extreme cases even ultra-relativistic.

The gamma-ray flash GRB 170817A that accompanied the gravitational wave signal GW 170817 (for reviews see Nakar 2020; Margutti & Chornock 2021) is a plausible example of a shock breakout signal (e.g., Kasliwal et al. 2017; Gottlieb et al. 2018b; Beloborodov et al. 2020); the RMS in this source was most likely driven by the interaction of the relativistic jet expelled by the compact remnant and the merger ejecta (Nakar et al. 2018), but a shock

with a much wider opening angle is also a viable possibility (Beloborodov et al. 2020). While the origin of GRB 170817A is still debatable, the presence of a relativistic jet in this system has been confirmed by VLBI observations (Mooley et al. 2018). Consequently, if this system represents a prototypical BNS merger evolution, the conclusion that a fast shock must cross through at least part of the ejecta at early times seems unavoidable. In what follows we demonstrate that the propagation of the RMS through the merger ejecta can significantly alter the composition profile of r-process material behind the shock and, potentially, the kilonova emission if the change in composition affects the opacity and/or the radioactive energy deposition in the ejecta.

A key issue in RMS theory is how the different plasma constituents are coupled. Since the radiation force acts solely on electrons and positrons, it must be mediated to the ions by some other means. In a sub-relativistic, single-ion RMS this is accomplished through the generation of an electrostatic field, owing to a tiny charge separation of electrons and ions. However, electrostatic coupling fails in relativistic RMS (RRMS), in which e^\pm pairs are overabundant (Levinson 2020; Vanthieghem et al. 2022), and in RMS composed of multi-ion species with different charge-to-mass ratios (Derishev 2018; Levinson et al. 2023). It has been shown recently (Vanthieghem et al. 2022) that in an unmagnetized single-ion RRMS, the dominant coupling mechanism is plasma microturbu-

^{*} E-mail: alongranot1@mail.tau.ac.il

lence, generated by a current filamentation instability driven by the relative drift between the ions and the pairs. The presence of a strong enough (transverse) magnetic field in the upstream flow can give rise to magnetic coupling of pairs and ions which completely suppresses the instability (Mahlmann et al. 2023).

The situation can be vastly different in multi-ion RMS. First, the deceleration rate of ions inside the shock by an electrostatic field depends on the charge-to-mass ratio, and since the charge conservation condition in a multi-ion plasma is degenerate a large velocity separation between the different ions in the post-deceleration zone is, in principle, allowed (even in sub-relativistic RMS), provided that interspecies friction is ineffective. As shown below, in some cases binary Coulomb collisions effectively couple the ions while in others they are not and detailed calculations are needed to assess whether the relative drift established just downstream of the shock surpasses the barriers for inelastic nuclear collisions. Second, since the gyro-radius of an ion of mass Am_p is larger by a factor Am_p/Zm_e than that of an electron (or positron), much stronger magnetic fields may be needed to couple all ions. Such strong fields may not be present in most relevant systems. Third, in cases where Coulomb friction is ineffective and cannot suppress plasma instabilities, the coupling of different ions by plasma micro-turbulence would require generation of wave modes different than in a single-ion RRMS.

In this paper, we construct a semi-analytic, multi-ion RMS model and use it to compute the structure of a shock propagating in different environments, with emphasis on shocks propagating in the expanding ejecta of BNS mergers. We find that in *Newtonian* shocks binary Coulomb collisions effectively couple the ions, particularly heavy ions with large atomic numbers. However, the presence of positrons, anticipated in fast enough shocks, can lead to the separation of light ions (mainly helium in r-process ejecta) from the bulk of the heavy ions. In case of BNS mergers, We estimate that a shock moving at a velocity $\gtrsim 0.3c$ (where c is the light speed) in ejecta containing a substantial He abundance, can induce a considerable change in the composition of r-process material behind the shock through collisions of alpha particles with heavy ions. Moreover, the presence of sufficiently abundant free neutrons in the shock upstream should lead to fission through the capture of free neutrons, which do not experience a significant deceleration by the shock, by neutron-rich isotopes downstream of the shock. The activation energy for neutron-induced fission ranges from practically zero for ^{235}U to a peak of about 40 MeV for elements of mass number $A \approx 100$. Consequently, if the shock is driven into the ejecta while free neutrons are abundant (i.e., before nucleosynthesis freezeout), a considerable impact on the abundance evolution of r-process elements by neutron capture is anticipated prior to the kilonova emission in regions where the shock velocity $\gtrsim 0.2c$. These gross estimates are supported by detailed calculations presented below.

The plan of the paper is as follows: In Sec. 2 we introduce the Multi-ion RMS model. In Sec. 3 we provide analytic estimates of ion-ion collision energies and collision frequencies. In Sec. 4 we present numerical solutions of the shock equations in the absence of interspecies friction for different compositions of the upstream plasma. In Sec. 5 we modify the model to include Coulomb friction forces. In Sec. 6 we consider the effect of electron-positron pairs on the shock structure. In Sec. 7 we estimate the fission rate by capture of free neutrons. In Sec. 8 we discuss the applications to BNS mergers. A detailed derivation of the shock equations can be found in appendix A, followed by the inclusion of coulomb interactions detailed in appendix B.

2 THE MULTI-ION SHOCK MODEL

We construct a semi-analytic model for a Newtonian RMS that propagates in a neutral plasma consisting of electrons and a collection of ions having different charge-to-mass ratios. For simplicity, the shock is assumed to be infinite, planar and in a steady state. Adopting the approach of Blandford & Payne (1981a); Blandford & Payne (1981b), we employ the diffusion approximation to compute the transfer of radiation through the shock. A comparison of analytic solutions with full Monte-Carlo simulations (Ito et al. 2020) indicates that the diffusion approximation is quite accurate even at shock velocities $\lesssim 0.3c$ or so, justifying this treatment. In contrast to the single-fluid approach invoked in all previous Newtonian RMS models, in which all plasma constituents are assumed to be tightly coupled, here we self-consistently compute the electrostatic coupling between the electrons and ions, imposed by the charge separation induced by the relative drift between the different multi-fluid components. This is accomplished by solving the energy and momentum equations of the radiation and the multi-fluid plasma, together with Maxwell's equations, taking into account the electrostatic force acting on the charged fluids. Our treatment is similar to that adopted in Levinson (2020) for the single-ion relativistic RMS, but with modifications necessary for the inclusion of multi-ion species, and with the beaming approximation for the radiative transfer replaced by the diffusion approximation.

To simplify the analysis, we neglect pair creation and nuclear transmutations, although, as shown below, fission and fusion might be important in the immediate downstream of fast shocks. We emphasize that our main goal here is not to present detailed calculations of the composition profile behind the shock, but merely to demonstrate that a substantial change in composition is likely to occur. The neglect of pair production is justified for most exploding systems, but not for the extreme densities anticipated in BNS merger ejecta (see Sec. 8 for a detailed discussion). We tend to believe that inclusion of pair creation, while considerably complicating the solutions, will not alter significantly the essence of the results obtained with the simplified model constructed below. We intend to incorporate pair production into our model in a future publication.

Our analysis also ignores potential generation of plasma waves by ion beam instabilities. The resultant plasma microturbulence can provide additional coupling mechanism on microscopic scales, that might alter the ion velocity distribution in the immediate downstream. To gain some insight into the effect of such anomalous coupling, we incorporate, in Sec. 5, a phenomenological interionic friction model into the shock equations (apart from binary Coulomb collisions). In Sec. 8 we estimate the ratio between the radiation and kinetic scales, and discuss the implications for the anomalous coupling length. Based on this estimate, we speculate that for RMS in BNS mergers, anomalous coupling may not alter significantly the results obtained in Sec. 4.3 in the absence of anomalous friction. For other exploding systems the effect of plasma instabilities is unclear.

2.1 Governing equations

We solve the shock equations in the rest frame of the shock, in which the flow is steady. We choose a coordinate system such that the upstream flow moves in the positive \hat{x} direction. All fluid quantities are henceforth measured in the shock frame, unless otherwise stated. Let n_e denotes the electron density and β_e its velocity (in units of c), and n_α , β_α , Z_α , A_α the density, velocity, atomic number and mass number, respectively, of ion species α (here, $\alpha = \text{He, Au, etc.}$). The charge-to-mass ratio of the α ion is then Z_α/A_α . Since

our analysis ignores pair production and nuclear transmutation (although, as explained below, they might be important downstream), all particle fluxes must be conserved across the shock. In particular, $j_e \equiv n_e \beta_e = n_{e,u} \beta_u$ and $j_\alpha \equiv n_\alpha \beta_\alpha = n_{\alpha,u} \beta_u$, here subscript u labels fluid quantities far upstream of the shock. For the upstream conditions anticipated (at early times) in BNS merger ejecta all ions are likely to be fully ionized. Hence, Z_α is a constant for all α . Charge neutrality of the upstream plasma implies $\sum_\alpha Z_\alpha n_{\alpha,u} - n_{e,u} = 0$, from which one obtains the relation

$$\sum_\alpha Z_\alpha j_\alpha - j_e = 0, \quad (1)$$

that holds everywhere.

The radiation force inside the shock acts solely on the electrons. This leads to a relative drift between the electrons and the different ion species which, in turn, induces charge separation, $\rho_e = e(\sum_\alpha Z_\alpha n_\alpha - n_e) \neq 0$, and the consequent generation of an electrostatic field, $\mathbf{E} = E(x)\hat{x}$. The change of this electric field across the shock is governed by Gauss' law:

$$\nabla \cdot \mathbf{E} = \frac{dE}{dx} = 4\pi\rho_e. \quad (2)$$

The last equation can be rendered dimensionless by transforming to the coordinate $d\tau = \sigma_T n_e dx$, here σ_T is the Thomson cross-section, and normalizing the electric field E by the fiducial field $E_0 = m_e c^2 j_e \sigma_T / e$, viz., $\tilde{E} = E/E_0 = eE/m_e c^2 j_e \sigma_T$. This yields

$$\frac{d\tilde{E}}{d\tau} = \chi \left(\sum_\alpha \frac{Z_\alpha j_\alpha \beta_e}{j_e \beta_\alpha} - 1 \right), \quad (3)$$

with

$$\chi = \frac{4\pi e}{\sigma_T E_0} \approx 10^{12} \left(\frac{n_{e,u}}{10^{25} \text{ cm}^{-3}} \right)^{-1} \beta_u^{-1}. \quad (4)$$

The density is normalized here to the fiducial density anticipated in BNS merger ejecta about a second after the merger (Eq. 31). In SNe and GRBs the anticipated density is much smaller, $n_{e,u} \lesssim 10^{15} \text{ cm}^{-3}$.

The energy and momentum equations of the multi-fluid system are derived in appendix A under the assumption that the electron and ion fluids are cold. This simplifying assumption is justified by the fact that the pressure inside the shock is completely dominated by the diffusing radiation. In the dimensionless form, the reduced set of equations read:

$$\frac{d}{d\tau} (\beta_e + \pi_\gamma) = -\tilde{E}, \quad (5)$$

$$\frac{d}{d\tau} \beta_\alpha = \mu \frac{Z_\alpha \beta_e}{A_\alpha \beta_\alpha} \tilde{E}, \quad (6)$$

$$\frac{d}{d\tau} \pi_\gamma = \frac{1}{\beta_e} \frac{d}{d\tau} (4\pi_\gamma \beta_e - \frac{d}{d\tau} \pi_\gamma), \quad (7)$$

where π_γ is the normalized radiation pressure, $\pi_\gamma = p_\gamma/m_e c^2 j_e$, and $\mu = m_e/m_p$ is the electron-to-proton mass ratio. Equations (3)-(7) form a closed set that can be solved once the values of β_u , j_e , j_α and Z_α/A_α are specified. The far upstream value of the electric field is $\tilde{E}(x \rightarrow -\infty) = 0$.

2.2 Numerical integration

Solutions for the multi-fluid RMS structure of a shock that propagates in photon-poor upstream are obtained in section 4 by numerically solving Eqs. (3)-(7), assuming a cold, neutral plasma in the far

upstream. We note that the shock equations, Eqs. (3)-(7), are invariant under translations, hence, the location of the origin can be chosen arbitrarily. For convenience, we start the integration in all runs at $\tau = 0$, with $\beta_{e,u} = \beta_{\alpha,u} = \beta_u$, $\pi_{\gamma,u} = 0.001$, $\tilde{E} = 0$, and $\tilde{T}_{\gamma,u}^{0x} = 0$ as initial values (at $\tau = 0$), where \tilde{T}^{0x} is the radiation energy flux, defined in Eq. A2. With this choice the radiation force at $\tau = 0$ is given by

$$\frac{d\pi_{\gamma,u}}{d\tau} = 4\pi_{\gamma,u}\beta_u = 0.004\beta_u. \quad (8)$$

We verified that as long as $\pi_{\gamma,u}$ is small enough (i.e., the upstream is photon poor), the solution converges, except for a shift in the location of the shock which, as explained above, is arbitrary.

Since only the ratio $j_\alpha/j_e = n_{\alpha,u}/n_{e,u}$ appears in the above equations, we find it convenient to normalize the upstream densities to the electron density $n_{e,u}$, and define $\tilde{j}_\alpha = j_\alpha/j_e$. To save computing time, we use $\chi = 10^6$ instead of the more realistic value given in Eq. (4). We checked that the solution is highly insensitive to the value of χ , provided it is not too small ($> 10^3$ roughly).

3 ESTIMATION OF ION-ION COLLISION ENERGY AND COLLISION FREQUENCY

A qualitative description of the multi-flow dynamics inside the shock is as follows: At the outset of the shock transition layer, the incoming electron fluid is decelerated and thus compressed, by the radiation force (the gradient of the radiation pressure in the diffusion limit). This creates charge separation which, in turn, induces an electrostatic field inside the shock. This electric field tends to decelerate the ions and accelerate the electrons, thereby providing coupling of the various plasma components. Charge neutrality is regained once the radiation pressure saturates (and the radiation force vanishes), completely suppressing the electric field. In the absence of any other coupling mechanism (e.g., binary collisions, plasma turbulence; see section 5 for further discussion), relative drifts between ions with different charge-to-mass ratio ensues in the post-deceleration zone (immediate downstream), depending on the value of Z_α/A_α . The slowest ion in the immediate downstream, which we henceforth term 'agile', is the one with the largest Z/A ratio among all ions present in the upstream flow.

While the full shock structure can only be found upon numerical integration of Eqs. (3)-(7), an expression for the immediate downstream velocity of each ion in terms of the electric potential across the shock can be obtained analytically by integrating Eq. (6) alone. This enables reasonably accurate estimates of the relative drift between the ions in the absence of effective friction and the consequent collision energies. In what follows, we provide estimates of the relative drifts, collision energies, and collision frequencies of ions in the immediate downstream when inter-species friction is ignored.

3.1 Ion velocity separation

Since ions do not experience the radiation force in our model, the change in their energy across the shock must equal the work done by the electrostatic field. When normalized to the upstream baryon energy, $m_p c^2 \beta_u^2 / 2$, the latter reads:

$$w_E \equiv \int_{-\infty}^{\infty} \frac{2E \cdot e}{m_p c^2 \beta_u^2} dx. \quad (9)$$

Integrating Eq. (6), an expression for the downstream terminal

velocity of ion species α is obtained in terms of w_E :

$$\beta_{\alpha,d} = \beta_u \sqrt{1 + w_E \frac{Z_\alpha}{A_\alpha}}. \quad (10)$$

The velocity difference between ion species α and α' now reads:

$$\Delta\beta_{\alpha,\alpha'} = \beta_u \left[\sqrt{1 + w_E \frac{Z_\alpha}{A_\alpha}} - \sqrt{1 + w_E \frac{Z_{\alpha'}}{A_{\alpha'}}} \right]. \quad (11)$$

This relation is exact, but the value of w_E is unknown. To estimate w_E we note that for the agile ion, the one with the largest charge to mass ratio, $\beta_{\text{agile},d}^2 < \beta_u^2$. Adopting $\beta_{\text{agile},d} = 0$ in Eq. (10) gives $w_E \approx -\frac{A_{\text{agile}}}{Z_{\text{agile}}}$. Substituting the latter expression into Eq. (11), we can evaluate $\Delta\beta_{\alpha,\alpha'}$ for all ions once the ratio $A_{\text{agile}}/Z_{\text{agile}}$ is specified.

As an example, consider a mixture of hydrogen and helium only. The agile ion here is H , for which $A_H/Z_H = 1$ and $w_E \approx -A_H/Z_H = -1$, giving $\Delta\beta_{He,H} \approx 0.21(\beta_u/0.3)$. This result is in good agreement with the numerical solution derived in section 4 (see Fig. 1), for which $\Delta\beta_{He,H} \approx 0.173$, for a shock velocity of $\beta_u = 0.3$. In the case of heavy r-process composition (section 4.3), we find $w_E \approx -A_{He}/Z_{He} \approx -2$ for the agile ion He . This yields, for example, velocity separation of $\Delta\beta_{Ga,He} \approx 0.095(\beta_u/0.3)$ between Ga (with $Z_{Ga} = 31$ and $A_{Ga} = 69$) and He , again in good agreement with the numerical solution ($\Delta\beta_{Ga,He} \approx 0.091$) presented in Fig. 3. We find good agreements in all other cases tested and conclude that Eq. (11) can be safely used to calculate relative drifts between ions.

The above derivation suggests that the downstream conditions are highly insensitive to the upstream density of the agile ion. As will be shown in Sec. 4, this may be of utmost importance for astrophysical applications. To see this, note first that Eq. (10) yields the exact result $w_E = -(A_{\text{agile}}/Z_{\text{agile}})[1 - (\beta_{\text{agile},d}/\beta_u)^2]$, which depends on $\beta_{\text{agile},d}$ to second order. From Eq. (10) we also deduce that the downstream velocity of the non-agile ions, for which $\beta_{\alpha,d} \gg \beta_{\text{agile},d}$, depends on $\beta_{\text{agile},d}$ to the same order, and since the flux j_α is conserved across the shock, the downstream density, $n_{\alpha,d} = j_\alpha/\beta_{\alpha,d}$, also depends on $\beta_{\text{agile},d}$ to second order. From Eqs. (5) and (7) we find, upon neglecting the electron contribution to the energy budget:

$$m_p c^2 \beta_u^2 w_E = 8e \int_{-\infty}^{\infty} E(x) \frac{\beta_{e,d}}{\beta_e(x)} dx.$$

Since to order $O(\beta_{\text{agile},d}/\beta_u)^2$ the left hand side of this equation is constant, it implies that $\beta_e(x)$ and, hence, $\beta_{e,d}$ and $n_{e,d}$, must be preserved to the same order. The charge neutrality condition downstream, $Z_{\text{agile}} n_{\text{agile},d} = n_{e,d} - \sum_{\alpha \neq \text{agile}} Z_{\alpha,d} n_{\alpha,d}$, then implies that the downstream density of the agile ion, $n_{\text{agile},d}$, must also be preserved to this order and is, therefore, highly insensitive to the upstream density $n_{\text{agile},u}$. In other words, the compression ratio of the agile ion increases as its mass fraction upstream decreases in order to maintain $n_{\text{agile},d}$ at the level required for charge neutrality downstream. This argument applies provided the diffusion approximation remains valid.

3.2 Collision energy

In order to compute the collision energy in $\alpha - \alpha'$ collisions, it is convenient to transform to the center of momentum frame (COM). One then finds

$$E_{COM} = \frac{1}{2} \frac{A_\alpha A_{\alpha'}}{A_\alpha + A_{\alpha'}} m_p c^2 \Delta\beta_{\alpha,\alpha'}^2, \quad (12)$$

where $\Delta\beta_{\alpha,\alpha'}$ is given by Eq. (11). As an example, consider the $H - He$ collision. With $A_H = 1, A_{He} = 4$, Eq. (11) yields $\Delta\beta_{H,He} =$

$0.17(\beta_u/0.3)$, and from Eq. (12) we have $E_{COM} = 11.5(\beta_u/0.3)^2$ MeV.

In general, we find that for light elements $E_{COM} \sim (1 - 20)(\beta_u/0.3)^2$ MeV and for heavy elements $E_{COM} \sim (10 - 300)(\beta_u/0.3)^2$ MeV. Thus, at shock velocities $\beta_u \gtrsim 0.5$, the collision energy can exceed ~ 1 GeV for certain combinations of ions.

Coulomb barriers range between about 1 and 300 MeV for most elements. Therefore, ion-ion collisions behind a fast enough shock may conceivably cause significant composition change.

3.3 Collision rate

The geometrical cross-section for inelastic collisions of ion species α and α' is given approximately by

$$\sigma_{\alpha,\alpha'} = \pi[(A_\alpha^{1/3} + A_{\alpha'}^{1/3})r_p]^2 \approx 0.068\sigma_T(A_\alpha^{1/3} + A_{\alpha'}^{1/3})^2, \quad (13)$$

where $r_p \sim 0.43 r_e \sim 1.2 fm$, with $r_e = \frac{e^2}{m_e c^2}$ being the classical electron radius, and $\sigma_T = \frac{8\pi}{3} r_e^2$ the Thomson cross section (e.g., Bass 1973; Kox et al. 1987).

The corresponding collision frequency is given by

$$\nu_{\alpha\alpha'} = n_{\alpha',d} \sigma_{\alpha,\alpha'} c |\Delta\beta_{\alpha,\alpha'}|. \quad (14)$$

To obtain the total collision frequency, we integrate over all $\alpha - \alpha'$ interactions with minimal energy E_{min} . This corresponds to a region in the shock with $\Delta\beta_{\alpha,\alpha'} > \sqrt{\frac{2(A_\alpha + A_{\alpha'})E_{min}}{A_\alpha A_{\alpha'} m_p c^2}}$. We use the coulomb barrier between any two nuclei as the minimal value. E_{min} is obtained by Eq. (1) in Royer et al. (2021).

The mean number of interactions, within the relevant region $\Delta\tau$, for ion of type α upon ion of type α' is:

$$\begin{aligned} \Delta\tau_{\alpha,\alpha'} &= \int_{\Delta\tau} \frac{\nu_{\alpha\alpha'} l_T}{\beta_{\alpha,d} \cdot c} d\tau = \int_{\Delta\tau} \frac{n_{\alpha',d} 0.068 \sigma_T (A_\alpha^{1/3} + A_{\alpha'}^{1/3})^2}{n_e \sigma_T} \cdot \frac{|\Delta\beta_{\alpha,\alpha'}|}{\beta_{\alpha,d}} d\tau \\ &= 0.068 \int_{\Delta\tau} \tilde{j}_{\alpha'} \frac{\beta_e}{\beta_{\alpha',d}} \cdot \frac{|\Delta\beta_{\alpha,\alpha'}|}{\beta_{\alpha,d}} (A_\alpha^{1/3} + A_{\alpha'}^{1/3})^2 d\tau \\ &= 0.068 \cdot (A_\alpha^{1/3} + A_{\alpha'}^{1/3})^2 \tilde{j}_{\alpha'} \int_{\Delta\tau} \beta_e \left| \frac{1}{\beta_{\alpha',d}} - \frac{1}{\beta_{\alpha,d}} \right| d\tau. \end{aligned} \quad (15)$$

We used $l_T = (\sigma_T n_e)^{-1}$.

4 NUMERICAL RESULTS

In this section, we present the solution of the shock equations, Eqs. (3)-(7). To illustrate the basic properties of the solution we begin with a simple example of a pure hydrogen-helium ($H - He$) mixture. We then present solutions for solar composition and for r-process elemental abundances anticipated in BNS merger ejecta. In all of these examples, the shock velocity is taken to be $\beta_u = 0.3$. The same case studies will be employed in subsequent sections, where friction (Sec. 5) and pairs (Sec. 6) will be included in the model, changing the shock structure in different regimes.

4.1 $H - He$ mixture

In our first example, we compute the structure of a shock propagating at a velocity $\beta_u = 0.3$ in a medium composed of $H - He$ mixture, with relative abundances of $X = 0.75, Y = 0.25$. With our normalization, this translates to the far upstream values $\tilde{j}_{H,u} = \frac{6}{7}$ and

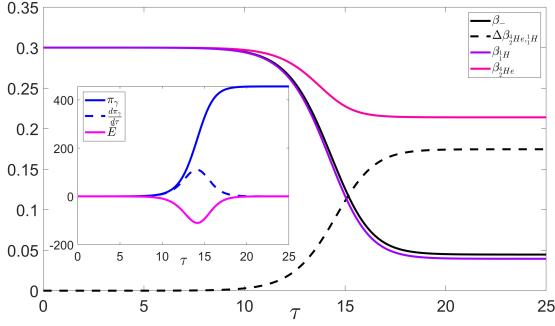
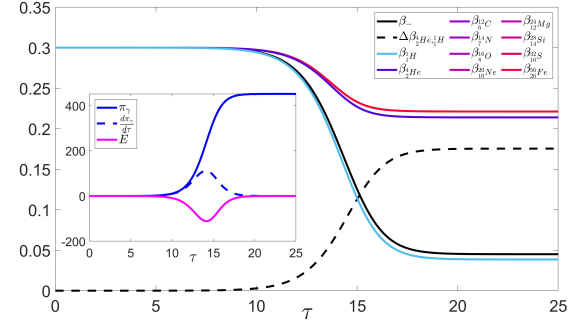


Figure 1. Shock structure solution obtained for a pure hydrogen-helium mixture. The solid blue and red lines represent the velocity profiles of H and He , respectively, as indicated, and the solid black line the velocity profile of the electrons. The black dashed line delineates the relative drift velocity $\Delta\beta_{He,H} = \beta_{He} - \beta_H$. The inset shows the electric field (red line), radiation force (blue dashed line) and radiation pressure (blue solid line). As seen, the relative drift velocity approaches $\Delta\beta_{He,H} = 0.173$ in the post-deceleration zone, at $\tau = 17$ roughly, where the electric field and radiation force vanish.

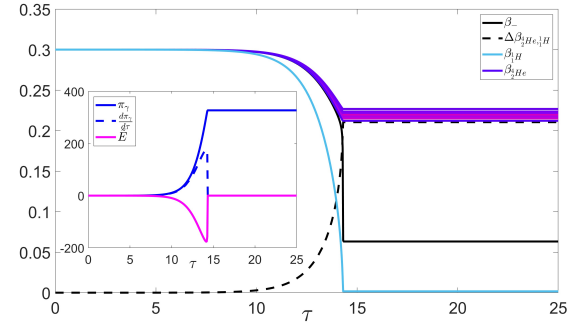
$\tilde{j}_{He,u} = \frac{1}{14}$ of H and He fluxes, respectively. The resultant shock structure is depicted in Fig 1. As seen, the small radiation force invoked at $\tau = 0$, Eq. (8), leads initially to the deceleration of the electrons, and the consequent generation of a negative electric field (magenta line in the inset) by the resultant charge separation. This electric field, in turn, decelerates the ions (Eq. 6), and counteracts the radiation force acting on the electrons (Eq. 5). As a result, the agile H ions remain tightly coupled to the electrons, owing to their larger charge-to-mass ratio, whereas the He ions quickly decouple. Charge neutrality is eventually regained (at $\tau \approx 17$), whereupon the net force acting on the system (the sum of electric and radiation forces) vanishes, and the plasma continues to stream undisturbed. The relative drift velocity (marked by the dotted black line) approaches $\Delta\beta_{H,He} = 0.173$ in the post deceleration zone, and the corresponding collision energy is ~ 12.16 MeV.

4.2 Solar abundances

In our second case, we use the solar elemental abundances given in Lodders (2019) (see Table 4 there). Figure 2a shows the shock profile. In similarity to the previous example, the hydrogen fluid remains tightly coupled to the electron fluid throughout the shock, but all other ions decouple and form a separate component, with a velocity spread considerably smaller than the relative drift between the H ions and all other ions. The collision energies range between practically zero and 20 MeV, for the shock velocity adopted, and are dominated by collisions of hydrogen with heavy ions. Above roughly 5 – 10 MeV, proton capture reactions for many elements (e.g. C, N and O) are quite rapid, with cross sections in excess of 100 mb (Soppera et al. (2012)). We thus anticipate such reactions to ensue at shock velocities $\beta_u \gtrsim 0.2$, provided that the relative velocity drifts are maintained for distances comparable to the shock width. While there is no detectable signature of H in the spectra of type Ib/c SNe, the progenitors of these SNe might nonetheless contain a small fraction of H (Hachinger et al. 2012). In fact, a study of the confirmed single type Ib progenitor that was detected in pre-explosion images (SN iPTF13bvn), suggests that H constitutes almost 1% of the progenitor’s mass (Gilkis & Arcavi 2022). Most of the H mass resides in the outer part of the envelope, where its fraction can reach tens of percents. We therefore considered also cases



(a) $X_H = 0.75$



(b) $X_H = 0.01$

Figure 2. Solutions for a shock with solar composition for different hydrogen mass fraction (X_H). The large difference in Z/A between the hydrogen and all other ions creates a clear distinction between the H fluid and the cluster of all other ions.

with relative H abundance substantially smaller than solar, specifically, in the range $10^{-5} - 1$ solar (Figure 2b). We find that over this range the ratio between the downstream densities of H and the remaining elements is practically independent of the mass fraction of H ahead of the shock. As explained at the end of Sec. 3.1, this is a consequence of the charge neutrality condition and the fact that the agile ion is most affected by the electrostatic field inside the shock.

In type Ib SNe, velocities of $0.1 \sim 0.15c$ may be obtained at the ejecta front (Chevalier & Soderberg 2010), which is marginal for proton capture. However, considerably higher shock velocities are conceivable in Type Ib/c, and if indeed contains H ions, proton capture reactions might be important in those systems, and can alter the composition in regions where the shock is fast enough.

4.3 r-process composition in BNS mergers

As a final (and most interesting) example we consider a shock propagating in BNS merger ejecta consisting of r-process material. The composition of various fluid elements in the ejecta of BNS merger depends on its initial condition, mostly the initial electron-fraction and its expansion velocity. However, all fluid elements have in common a dominant fraction of r-process material, free neutrons (which we include later in Sec. 7), and a non-negligible fraction of He. Since He is the most agile element expected in the ejecta, its presence has a significant effect on the velocity spread. Typical He mass fractions found in various simulations range between 10^{-4} and 0.1 (Tarumi et al. 2023 and references therein). We calculated the velocity spread for far-upstream compositions with these two extreme

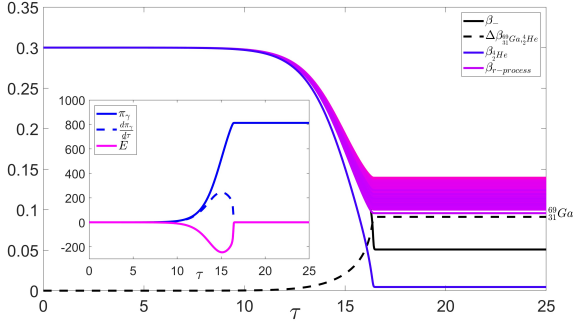


Figure 3. Same as Fig. 2 for a shock propagating in a BNS merger ejecta, containing He ions with a mass fraction of $X_{He} = 10^{-2}$. The ${}^{69}_{31}\text{Ga}$ ions represent the r-process span, having the lowest downstream velocity.

values, whereas for the r-process elements we adopt the abundances given by [Goriely \(1999\)](#).

The results are summarized in Fig. 3, where we use the mass number A instead of Z to label the different ions, since different isotopes of the same elements are present in the system. The He mass fraction in this example is $X_{He} = 10^{-2}$. As in the case of solar abundance with varying X_H , we find that in the range $10^{-4} < X_{He} < 0.1$ that we explored, the ratio between the density of He and the remaining elements in the immediate downstream is independent of the mass fraction of He ahead of the shock. Nearly all elements would experience collisions with He with COM energies well above the Coulomb barrier. This should give rise to nuclear transmutations of many isotopes at shock velocities $\beta_u \gtrsim 0.2$,

5 INCLUSION OF INTERIONIC FRICTION

Momentum exchange between the different plasma beams can transfer the radiation force to the ions, ultimately leading to coupling of all plasma constituents. Binary Coulomb collisions constitute one potential mechanism for such interspecies friction. In situations in which this mechanism fails to strongly couple the ions preventing large relative drifts, it is expected that the velocity distribution of the multi-ion plasma established in the post-deceleration zone (Figs 1-3) will be prone to various beam instabilities. This would result in the generation of plasma microturbulence that can transfer momentum between different ion beams via ion scattering off plasma waves, thereby driving the downstream plasma towards equipartition. The anomalous coupling length is expected to depend on the threshold drift velocity for the onset of the instability, on the saturation level of the turbulence, and conceivably other factors. Moreover, the continuous decrease of the relative drift velocity between different ion species will induce charge separation that will affect the electrostatic field. We note that conversion of the dissipation energy to radiation can only occur over the radiation length scale. Consequently, if the anomalous coupling length is much smaller than the Thomson length, dissipation via anomalous friction should first lead to ion heating before the energy will be converted to radiation. (On a global scale this would appear as formation of collisionless subshocks.) Furthermore, if the growth of the instability occurs well after decoupling, the ion temperature should be high enough to allow inelastic ion-ion collisions by random motions. On the other hand, the electrostatic field induced by the interionic friction may prevent the early decoupling of ions with small Z/A seen in the solutions presented in Sec. 4, thereby suppressing the rate of inelastic ion-

ion collisions. What would actually happen depends, ultimately, on the threshold velocity of the instability and the scale separation. In Sec. 8 we provide a rough estimate of the scale separation in RMS, and conclude that in BNS mergers the anomalous coupling length is likely to be comparable to, or even larger than, the radiation length, whereas in other systems it is most likely much smaller. Thus, the situation might be different in different types of systems.

To gain insight into the effect of interionic friction, we constructed, in Sec. 5.1, a (simplified) phenomenological friction model meant to represent unspecified anomalous coupling mechanism. The model ignores any threshold effects, and doesn't take into account ion heating, thus, it is rather limited. Nonetheless, it elucidates some basic features that can guide future analysis. In Sec. 5.3 and appendix B we derive friction coefficients for binary Coulomb collisions, and present shock solutions that incorporate Coulomb friction between all species.

5.1 A phenomenological friction model

The full derivation of the shock equations with interspecies friction is given in appendix A1. Here we provide a succinct account of the friction model. We suppose that the change in momentum of ion α due to momentum exchange with ion beam α' is proportional to the relative velocity between ion species α and α' , and the density of the α' beam: $\mathcal{F}_{\alpha\alpha'} = -g_{\alpha\alpha'} n_{\alpha'} (\beta_\alpha - \beta_{\alpha'})$, where $g_{\alpha\alpha'}$ is a characteristic friction coefficient. Momentum conservation requires the symmetry $g_{\alpha\alpha'} = g_{\alpha'\alpha}$ (see A1 for details). The total friction force exerted on ion α is the sum over all ion beams. In terms of the conserved fluxes \tilde{j}_α and the coordinate τ , the modified Eq. (6) reads:

$$\frac{d}{d\tau} \beta_\alpha = \frac{\beta_e}{\beta_{\alpha A \alpha}} \left[\mu \tilde{E} Z_\alpha - \sum_{\alpha'} \tilde{g}_{\alpha\alpha'} \frac{\tilde{j}_{\alpha'}}{\beta_{\alpha'}} (\beta_\alpha - \beta_{\alpha'}) \right], \quad (16)$$

here $\tilde{g}_{\alpha\alpha'} \equiv \frac{g_{\alpha\alpha'}}{m_p \sigma_T}$ defines a dimensionless friction coefficient. In what follows we assume for simplicity that all the coefficients are equal: $\tilde{g}_{\alpha\alpha'} = \tilde{g}$. This, of course, may not be realistic in practice (and indeed not the case for, e.g., Coulomb collisions; see Sec. 5.3). Nonetheless, it allows us to estimate the strength of the friction force required to tightly couple all ions.

As stated above, momentum conservation is automatically satisfied if the coefficients $g_{\alpha\alpha'}$ are symmetric. However, since friction forces are dissipative, additional physics is needed to specify how the dissipation energy is distributed. Here, we assume that energy is transferred from ions to electrons over a length scale sufficiently short to keep the electron and ions fluids cold (i.e., highly supersonic) at all times. Under this assumption the energy equation reduces to Eq. (A11) in appendix A1.

5.2 Shock solutions

Replacing Eq. (6) with Eq. (16), we obtained new solutions for the shock structure. Results for the $H - He$ and r-process compositions are shown in Fig. 4 and Fig. 5 respectively. We find no effect on the shock structure up to $\tilde{g} \lesssim 10^{-2}$ (10^{-1} for the r-process case). At $\tilde{g} \sim 10^{-1}$ (10^0), the friction force succeeds to couple all the components together on length scales of a few l_T , yet enabling ion-ion collisions. For $\tilde{g} > 1$ (10^2) no velocity differences are obtained and the shock acts as a single fluid.

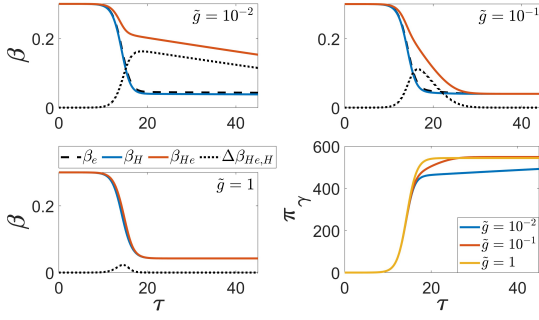


Figure 4. Shock solutions for a pure $H-He$ composition, as in Fig. 1, and different values of the friction coefficient \tilde{g} , as indicated. The lower-right panel displays the radiation pressure profile for the three cases presented in the other panels ($\tilde{g} = 10^{-2}, 10^{-1}, 1$). As seen, full coupling occurs for $\tilde{g} \geq 1$.

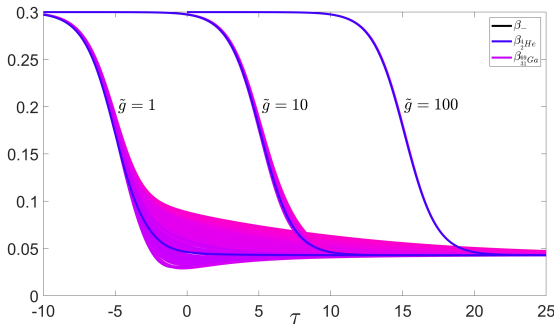


Figure 5. Shock solutions for r-process composition (same as in Fig. 3) with constant friction coefficient of $\tilde{g} = 10^0, 10^1$, and 10^2 , as indicated. The different plots are shifted by $\Delta\tau = 10$ for visualization purposes.

5.3 Coulomb friction

Friction via binary Coulomb collisions between different ion species and between ions and electrons was previously considered by Weaver (1976) based on Spitzer’s formula. These interactions strongly depend on the relative velocity between the colliding species as $\propto v^{-3}$, which can be dominated by either the relative drift or thermal motions. Since our model does not contain a self-consistent treatment of photon generation inside the shock, we are unable to determine the temperature along the shock transition layer. Instead, we invoke a constant temperature, $k_B T \equiv \theta m_e c^2$, which is treated as a free parameter. We obtain solutions for a relevant range of temperatures found in detailed Monte-Carlo calculations of single fluid shock models (see Ito et al. 2020; Levinson & Nakar 2020).

The detailed derivation of the Coulomb friction coefficients is presented in appendix B. Unlike the constant coefficients of the phenomenological friction model adopted in §5.1, the Coulomb friction coefficients are characterized by a cubic dependence on the relative velocity of the colliding ions (including the thermal spread) and their atomic charge and mass:

$$\tilde{g}_{aa'} = \frac{\mu^2}{\sqrt{2\pi}} \frac{A_a + A_{a'}}{A_a A_{a'}} Z_a^2 Z_{a'}^2 \frac{\ln \Lambda_{aa'}}{\Delta\beta_{aa'}^3}. \quad (17)$$

Here the subscripts a and a' denote either ions (with subscript α , atomic number Z_α and mass number A_α) or electrons (with $A_e = \mu, Z_e = -1$), $\ln \Lambda_{aa'}$ is the Coulomb logarithm, given explicitly in Eq. (B3), and $\Delta\beta_{aa'}^2 = \Delta\beta_{drift,aa'}^2 + \Delta\beta_{thermal,aa'}^2$, is the sum of

the relative drift, $\Delta\beta_{drift,aa'}^2 = (\beta_a - \beta_{a'})^2$, and the thermal speeds, $\Delta\beta_{thermal,aa'}^2 = 2kT_a/m_a c^2 + 2kT_{a'}/m_{a'} c^2$. For simplicity, we shall henceforth assume that all species have the same temperature, measured in $m_e c^2$ units, $\theta = kT/m_e c^2$, in which case $\Delta\beta_{thermal,aa'}^2 = 2\mu\theta(A_a + A_{a'})/A_a A_{a'}$. Eq. (17) indicates a strong dependence on the atomic numbers, implying that the friction force is expected to be much stronger for heavy elements than for light elements. Shock solutions with Coulomb friction are obtained upon substituting the Coulomb friction coefficients, Eq. (17), into Eq. (16).

A general expression for the ratio between the Coulomb friction coupling length, $l_{aa'}$, and the shock length, $l_{sh} = (\beta_u n_e \sigma_T)^{-1}$, is given in Eqs. (B8) and (B9). First, we consider Coulomb coupling between ions and electrons in a kilonova. Taking $n_e = 10^{25} \text{ cm}^{-3}$ and $\theta = 0.1$ as characteristic values, we obtain that for coupling of r-process elements to electrons $\ln \Lambda_{\alpha e} \approx 10$, and:

$$l_{\alpha e, KN} \approx 0.1 \cdot \beta_{u,0.3}^2 \theta_{0.1}^{3/2} Z_{\alpha,50}^{-1} l_{sh}, \quad (18)$$

The coupling length between electrons and lighter elements, such as He, is longer due to their lower charge:

$$l_{He,e,KN} \approx 3 \cdot \beta_{u,0.3}^2 \theta_{0.1}^{3/2} l_{sh}, \quad (19)$$

The assumption that the thermal velocity is larger than the drift velocity, which was used to derive Eqs. (B8) and (B9), is always satisfied for coupling with electrons at relevant KN conditions since $\Delta\beta_{thermal,\alpha e} \approx \sqrt{2\theta} \approx 0.4 \cdot \theta^{1/2} \gtrsim \beta_u$.

Next we consider the inter-ion coupling length. For a typical r-process nuclei α and α' we find $\ln \Lambda_{\alpha\alpha'} \approx 1$ and as long as the relative velocities are dominated by thermal motion, the coupling distance of a heavy nucleus α to the rest of the r-process elements is

$$l_{\alpha,KN} \approx \left(\sum_{\alpha' \neq \alpha} l_{\alpha\alpha',KN}^{-1} \right)^{-1} \approx 10^{-4} \cdot \beta_{u,0.3}^2 \theta_{0.1}^{3/2} A_{\alpha,100}^{-1/2} Z_{\alpha,50}^{-1} l_{sh}, \quad (20)$$

This coupling length holds as long as $\Delta\beta_{drift,\alpha,\alpha'} < \Delta\beta_{thermal,\alpha,\alpha'} \approx 0.001(\theta_{0.1}/A_{100})^{1/2}$ (see discussion below Eq. B8). If at some point within the shock transition layer the relative velocity, $\Delta\beta_{drift,\alpha,\alpha'}$ exceeds this value the coupling length depends on the drift instead of the thermal velocity, so $l_{\alpha,KN} \propto \Delta\beta_{drift,\alpha,\alpha'}^3$. In such case there is a run-away of the drift velocity and the coupling breaks. Approximating the drift velocity that develops within the shock transition layer, as long as the thermal velocity dominates over the drift velocity, as $\Delta\beta_{drift,\alpha,\alpha'} \sim \frac{\beta_u l_{\alpha,KN}}{\max\{l_{sh}, l_{\alpha'e,KN}\}}$ we obtain the following criterion for r -process elements with themselves:

$$\frac{\Delta\beta_{drift,\alpha,\alpha'}}{\Delta\beta_{thermal,\alpha,\alpha'}} \sim \beta_u \frac{l_{\alpha,KN}}{\max\{l_{sh}, l_{\alpha'e,KN}\}} \left(\frac{A_\alpha}{2\mu\theta} \right)^{\frac{1}{2}} \approx \begin{cases} 0.03 \cdot \beta_{u,0.3}^3 \theta_{0.1} Z_{\alpha,50}^{-1} & l_{\alpha'e,KN} < l_{sh} \\ 0.3 \beta_{u,0.3} \theta_{0.1}^{-1/2} & l_{\alpha'e,KN} > l_{sh} \end{cases}, \quad (21)$$

where the smallest of the two options always apply. Following the same argument for coupling of He to heavy ions we obtain $\ln \Lambda_{He,\alpha} \approx 10$, and:

$$l_{He,\alpha,KN} \approx \left(\sum_{\alpha' \neq He} l_{He,\alpha',KN}^{-1} \right)^{-1} \approx 0.01 \cdot \beta_{u,0.3}^2 \theta_{0.1}^{3/2} l_{sh}, \quad (22)$$

so the criterion for frictional coupling is

$$\frac{\Delta\beta_{\text{drift,He},\alpha}}{\Delta\beta_{\text{thermal,He},\alpha}} \sim \beta_u \frac{l_{\text{He},\alpha,\text{KN}}}{\max\{l_{\text{sh}}, l_{\alpha'e,\text{KN}}\}} \left(\frac{2}{\mu\theta}\right)^{\frac{1}{2}} \quad (23)$$

$$\approx \begin{cases} 0.75 \cdot \beta_{u,0.3}^3 \theta_{0.1} & l_{\alpha'e,\text{KN}} < l_{\text{sh}} \\ 0.3 \cdot \beta_{u,0.3} \theta_{0.1}^{-1/2} & l_{\alpha'e,\text{KN}} > l_{\text{sh}} \end{cases}$$

Eqs. 18, 19, 21 and 23 provide the coupling criteria of the various plasma constituents when only friction is at work. In reality, electrostatic field, as well as anomalous coupling, may also play a role. Applying these criteria to shocks in KN ejecta we find that the heavy r-process elements are tightly coupled and therefore behave as a single fluid (Eq. 21). The heavy element fluid is coupled to electrons via Coulomb friction (Eq. 18) with the assistance of electrostatic field. Finally, while the Coulomb coupling of He to the rest of the plasma elements is marginal, the electrostatic field guarantees strong coupling of the He as well. The result is that for the conditions expected in KN ejecta we expect all the plasma constituents to behave as a single fluid, at least as long as no pairs are present (see §6 for the effect of pairs). This expectation is verified by detailed calculations (see Fig. 6 for example).

For a supernova, taking $Z = \{1, 2\}$, $n_e = 10^{15} \text{ cm}^{-3}$ and $\theta = 0.01$, we find $\ln\Lambda_{\alpha\alpha'} \approx \ln\Lambda_{\alpha e} \approx 10$, and

$$l_{\alpha\alpha',\text{SNe}} \approx 10^{-3} \beta_{u,0.1}^2 \theta_{0.01}^{3/2} l_{\text{sh}}, \quad (24)$$

$$l_{\alpha e,\text{SNe}} \approx 0.01 \cdot \beta_{u,0.1}^2 \theta_{0.01}^{3/2} l_{\text{sh}}.$$

As seen, ion-ion collisions dominate the Coulomb friction force in this case as well and the electrostatic field guarantees coupling to the electrons when the ions behave as a single fluid. Equation (24) indicates that strong coupling is anticipated at not-too-high velocities. In fast enough shocks, $\beta \gtrsim 0.4$, where the temperature inside the shock exceeds $\sim 100 \text{ keV}$ (Ito et al. 2020; Levinson 2020), Coulomb friction alone may be insufficient to prevent velocity spread behind the shock (as we show later the formation of pairs at these temperature is expected to further reduce the coupling). An example of a shock solution with $\beta_u = 0.4$ and $\theta_e = 0.2$ is shown in Fig. 7. A relatively large drift between He and all other ions is observed (e.g. Fe, Si). The generation of plasma turbulence by ion beam instability, expected under such conditions, can accelerate particles and alter the breakout signal. The anomalous friction due to plasma turbulence will probably reduce the drift velocity, yet it may still be sufficient to ignite helium-induced γ emission as the shock passes through the star ($\text{He} + X \rightarrow \text{He}' + X' + \gamma$), and conceivably (though with a lower cross-section) alpha-capture ($\text{He} + {}^A_Z X \rightarrow {}^{A+4}_{Z+2} X + \gamma$).

5.4 Thermal effects

There are two temperature-related aspects, which we do not address in this work, that are predicted to contribute to the decoupling of the ions, and thus to the collision rate. First, since $l_{\alpha,\alpha'} < l_{\alpha,e}$ by a factor of μ , the ion temperature can potentially be higher than that of the electrons and the radiation along the shock transition layer. The reason is that the heating of the ions due to Coulomb collisions that are responsible for keeping them coupled within the shock transition layer (although each ion species decelerates at a different rate due to the electrostatic field), is done over $l_{\alpha,\alpha'}$. The transfer of this heat to the electrons and then to the photons, which dominates the heat capacity of the shock transition layer and the downstream, is done over $l_{\alpha,e}$. Thus, the ions and the electrons can have two distinct temperatures, where the former can, in some scenarios, be significantly

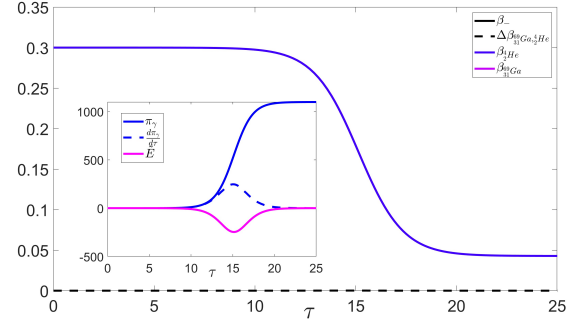


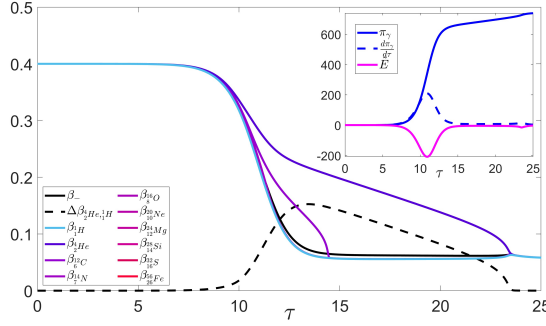
Figure 6. Shock structure for r-process composition with $\beta_u = 0.3$, $n_e = 10^{25}$ and $\theta = 0.2$. The strong coupling of all ions by Coulomb friction is clearly seen main panel.

higher than the latter. Increasing temperature will decrease the efficiency of inter-ion binary collision, increasing the coupling length. A second thermal effect is due to the thermal velocity dispersion within each beam. The collision rate is a function of the coupling length $l \propto E^{3/2}$ and the density, which, assuming a Maxwellian distribution for each ion species, is proportional to $\propto \sqrt{E} e^{-E/E_0}$. Integrating altogether, this effect gives a factor of ~ 2 to the total rate. We leave this, again, to future work.

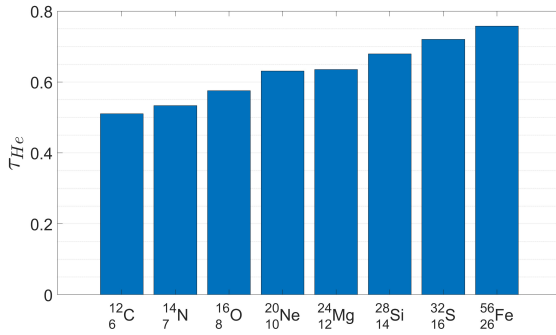
6 THE ROLE OF PAIRS

For shock temperatures exceeding $\sim 50 \text{ keV}$ ($\theta \sim 0.1$) pair production starts to play a role. This will be important at shock velocities $\beta_u \gtrsim 0.35$ for $n_e \sim 10^{15} \text{ cm}^{-3}$ and light element composition, and $\beta_u \gtrsim 0.25$ for $n_e \sim 10^{25} \text{ cm}^{-3}$ and heavy r-process element ejecta, corresponding to SNe and kilonova environments respectively (Levinson & Nakar 2020). The presence of positrons with larger than unity multiplicity can substantially affect the shock structure. First, positrons tend to decelerate faster than all other species since, in contrast to electrons, the electric and radiation forces acting on them are in the same direction, and they have a large charge to mass ratio, ~ 2000 . Thus, in the absence of tight coupling by friction, the positrons are strongly compressed and decouple from the other species early on, as shown by detailed calculations for relativistic RMS (Levinson 2020). Consequently, plasma instabilities should play important role and need to be taken into consideration. When the coupling between electrons and positrons by Coulomb friction is strong enough, complete screening of the electric field inside the shock ensues, considerably affecting the dynamics of alpha particles (see details below). Second, the larger the pair multiplicity, the larger the opacity for Thomson scattering, resulting in a smaller physical shock width. This can potentially alter the ratio between the radiation length and the coupling length of various ions.

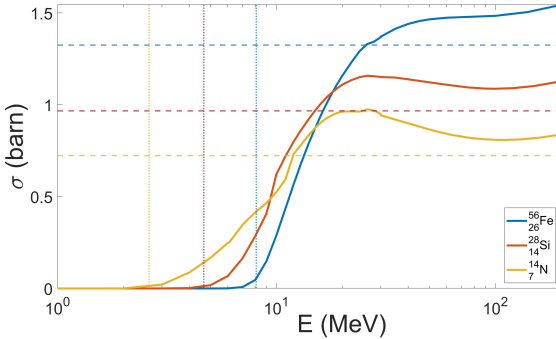
In order to accurately quantify these effects, self-consistent calculations of pair loaded multi-ion RMS is needed. This, in turn, requires a proper account of photon production processes in the model, which is beyond the scope of our current analysis. We leave the construction of a generalized model for future work. In what follows, we study the effect of pair loading using a simplified model. To be concrete, we assume that the upstream plasma contains electron positron pairs with a fixed multiplicity, $M \equiv n_{+,u}/(n_{e,u} - n_{+,u})$, where $n_{+,u}$ is the upstream positron density and $n_{e,u} = n_{+,u} + \sum_{\alpha} n_{\alpha,u} Z_{\alpha}$ is the total electron density, and ignore pair production inside the shock. With this definition we have $j_{+}/j_e = M/(M+1)$, where $j_{+} = n_{+}\beta_{+}$



(a) Shock structure for multi-ion solar-like ambient, including coulomb interactions, with $\beta_u = 0.4$, $n_e = 10^{15} \text{ cm}^{-3}$ and $\theta = 0.2$. The left panel shows the electric field and radiation pressure evolution. The right panel depicts the velocity profile of the different constituents. A relative drift of $\sim 0.15c$ is obtained giving rise to collision energies of $\sim 35 - 40 \text{ MeV}$.



(b) Non-elastic collision depth for different ions with ^4He within the shock. Cross sections are taken to be geometrical, and the length is calculated above the fusion barrier as explained below (c). roughly ~ 0.6 of all ions would interact with He ions.



(c) Non-elastic cross-sections for Fe , Si and N with He taken from <https://www-nds.iaea.org/exfor/endl.htm>. The geometrical cross-sections used in our estimations are calculated by $\sigma_{X(\text{He}, \text{non})} = 0.0452 \cdot (A_X^{1/3} + A_{\text{He}}^{1/3})^2 \text{ barn}$ and shown by the horizontal dashed lines in the matching colors. The fusion barriers we use are shown in the matching vertical dotted lines.

Figure 7.

(see next subsection). We explore solutions for a multiplicity range $M = 1 - 30$, as indicated by Monte-Carlo simulations for fast Newtonian RMS (Ito et al. 2020), taking into account Coulomb friction between all species. The corresponding equations are derived in appendix A2.

6.1 A simplified pair loaded multi-ion RMS model

Since our model ignores pair creation, the positron flux is conserved, $j_+ = n_+ \beta_+ = \text{const}$. The charge neutrality condition then generalizes to

$$\sum_{\alpha} j_{\alpha} Z_{\alpha} + j_+ = j_e. \quad (25)$$

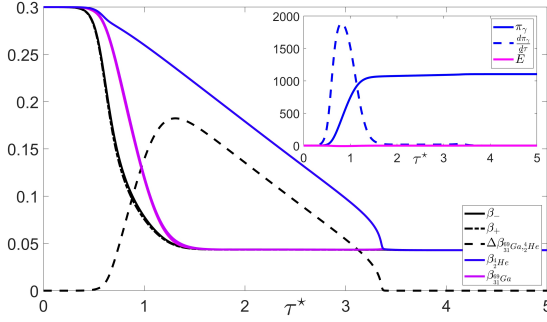
Since the radiation is coupled to positrons in addition to electrons, the advection of radiation in the shock depends on both β_e and β_+ , and Eq. (A1) is no longer valid. Henceforth, we assume that the advection velocity of the radiation field is given by $\beta_{adv} = (n_e \beta_e + n_+ \beta_+) / (n_e + n_+)$. As will be shown below, at multiplicities $M \gtrsim$ a few, the electron and positron fluids are strongly coupled, so that practically $\beta_{adv} = \beta_e$. The reason is that for $M > 1$ the electric field inside the shock is nearly completely screened, hence both fluids experience the same force (the radiation force) and, consequently, the same deceleration. With this choice of β_{adv} the energy flux of the radiation field is given by Eq. (A14), where τ is the optical depth contributed by the electrons, that is, $d\tau = \sigma_T n_e dx$.

Now, in the momentum equations, one should take into account the fact that the momentum transferred to the electron fluid by the radiation at any given position is proportional to the relative number of scatterings, $n_e / (n_e + n_+)$, and likewise for the positron fluid. Moreover, the friction forces associated with the positron fluid should also be accounted for. The resultant momentum equations are given in Eqs. (A15)-(A16). For the results presented below we assume that friction forces are solely due to binary Coulomb collisions, as in Sec. 5.3, but including the positron fluid. Specifically we add ion-pairs bilateral friction and present a new electron-positron friction given by Eq. (17) with $A_{\pm} = \mu$ and $Z_{\pm} = \pm 1$.

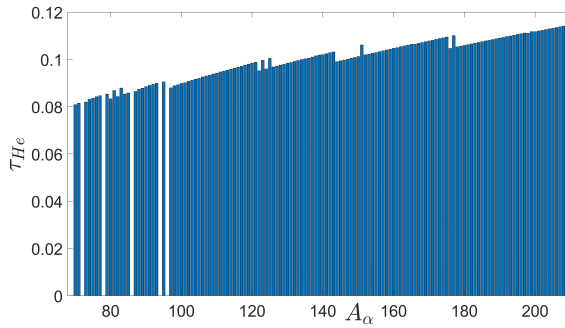
Two examples of pair loaded shock solutions are exhibited in Figs. 8 and 9. For comparison purposes the velocity profiles in these figures are plotted as functions of the pair unloaded optical depth, $d\tau^* = \frac{n_e}{1+M} \sigma_T dx$. Fig. 8a shows a solution of a shock with $M = 10$ propagating in r-process ejecta under the same conditions as in Fig. 6. As seen, while in the absence of pairs all species, including He ions, are fully coupled (Fig. 6), in the presence of pairs the He ions develop a large relative drift with respect to the remaining ion cluster (represented by the magenta line in Fig. 8a). This result can be understood by considering the effect of pairs on the ratio between the Coulomb friction length scale and the shock width. The shock width shrinks as $l_{sh} \propto M^{-1}$, and the Coulomb length scales for coupling of ions and electrons (as well as positrons) are also reduced by the same factor (M^{-1}). Consequently, Eqs. (18) and (19) are unaffected by the presence of pairs. Likewise, the ion-ion Coulomb length scale is not affected directly by pairs, however, the reduction of the shock width implies that the r.h.s in Eqs. (20)-(23) is multiplied by M . Similarly, in Eq. (24) the expression for $l_{\alpha\alpha', SNe}$ is multiplied by M on its r.h.s, while the expression for $l_{\alpha e, SNe}$ is unaffected by pairs.

We can now understand why the presence of pairs leads to the decoupling of the He. First, at the anticipated multiplicity, pairs screen nearly completely the electrostatic field, hence, in the absence of significant anomalous friction, the coupling is solely due to Coulomb friction. Eq. (18) implies that for mildly relativistic shocks the heavy ions are at least marginally bound to the pairs and therefore they are expected to follow the electrons either tightly or with a short lag. The He ions, however, are not bound to the electrons (Eq. 19) and for $M \gtrsim 5$ are also not expected to be bound to the heavy ions. We therefore expect that if $M \gtrsim 5$ within the shock transition layer then a significant drift velocity is developed between He and the heavy ions.

The separation of the He ions in Fig. 8a is large enough to al-



(a) Shock structure for pair-loaded r-process plasma with $M = 10$, $\theta = 0.2$ and $\beta_u = 0.3$. The helium mass fraction is 0.04, meaning one alpha particle per each heavy ion. For comparison with previous cases, the various profiles are plotted as functions of the pair unloaded optical depth, $d\tau^* = \frac{n_e}{1+M} \sigma_T dx$.



(b) Non-elastic collision depth for different heavy ions with 4He within the shock. Cross sections are taken to be geometrical, and the length is calculated above the fusion barrier. Roughly ~ 0.1 of all heavy ions would interact with He ions. Increasing the helium mass fraction to ~ 0.1 will increase the τ_{He} respectively to ~ 0.25 .

Figure 8.

low inelastic collisions with the heavy ions downstream. The optical depth for collisions above the Coulomb barrier of different ions is shown in the lower panel Fig. 8b for He mass fraction of $X_{He} = 0.04$. We find, as expected, that the probability for inelastic collisions is proportional to X_{He} . For $X_{He} = 0.1$, the highest value found in some simulations (Tarumi et al. 2023), our simplified model indicates that about 25% of the r-process isotopes will be converted through inelastic collisions with He ions in a shock moving at a velocity $\beta_u = 0.3$. The dependence of the He velocity separation on temperature and pair multiplicity necessitates a self-consistent treatment of pair-loaded shocks in order to assess more accurately the conditions under which significant nuclear transmutations by collisions of heavy ions with alpha particles is expected. We defer such analysis for future publication.

7 THE ROLE OF FREE NEUTRONS

The ejected material in BNS merger consists of various r-process isotopes, alpha particles, and free neutrons. The rapid neutron capture process lasts for about 1 sec before the mixture reaches freeze-out, followed by the decay of unstable isotopes into their final stable states, whereby the final composition of the r-process ejecta is gradually established. An example of the evolution of the r-process mixture is shown in Fig. 10.

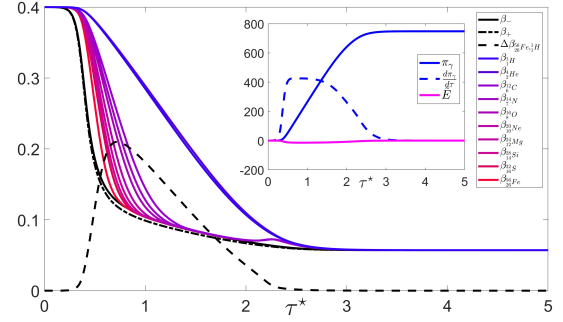


Figure 9. Shock structure for pair-loaded solar-like plasma with $M = 10$, $\theta = 0.2$ and $\beta_u = 0.4$

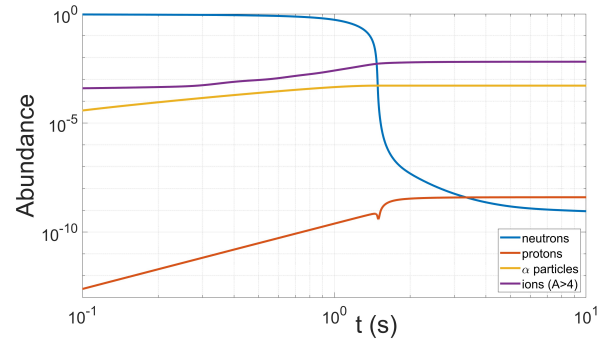


Figure 10. Abundance temporal evolution of the different constituents in a kilonova remnant around the “freeze-out” phase of the r-process (here freeze-out takes place roughly at 1.5s). The results were obtained using the “SkyNet” r-process module (Lippuner & Roberts 2017). The initial conditions are $Y_e = 0.01$, $T_0 = 6\text{ GK}$, $s = 10 \frac{k_B}{\text{baryon}}$ and $\tau_{exp} = 7.1\text{ ms}$.

If the shock crosses the ejecta early enough, a relatively large abundance of free neutrons may be present in the upstream region. One might naively suspect that free neutrons advected with the upstream flow will cross the shock undisturbed, and might trigger fission via various types of inelastic collisions with the shocked ions. However, there exist three main channels through which neutrons crossing the shock may interact with the ions inside the shock: elastic scattering ($nX, n'X'$), inelastic radiative scattering ($nX, n'X'\gamma$) and other non-elastic scattering processes, most of which results in nuclear transmutation (e.g., neutron capture, spallation, fission, etc.). A reaction that can induce nuclear transmutations requires the collision energy to exceed the activation barrier ($\lesssim 25$ MeV for most isotopes), while elastic collisions are effective also at low energies. Thus, if the elastic collision rate is shorter than the shock crossing time, it can couple the neutrons to the ions, preventing large velocity spreads.

Figure 11 shows the geometric (an approximation of the elastic), non-elastic and γ -emission cross-section. It shows that the latter is smaller by about two orders of magnitude compared to the other two, which are of the same order. In what follows, we explore whether elastic collisions can couple the neutrons to the ions within the shock transition layer, thereby avoiding large drift velocity between them, or whether the neutrons cross the shock almost unaffected.

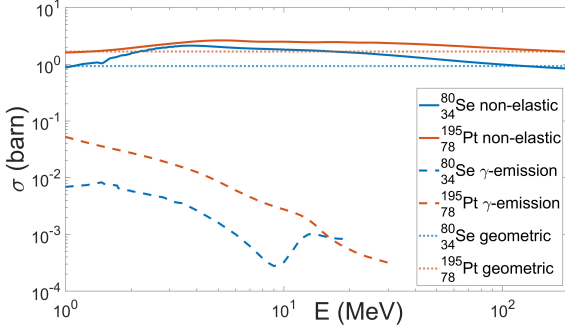


Figure 11. Total non-elastic, γ -emission and calculated geometric cross-sections for two representative isotopes (^{80}Se and ^{195}Pt) with incoming neutron for 1–200 MeV. γ -emission is only $\sim 1\%$ of total inelastic interactions, meaning ionic transmutations are probable. Data is taken from Evaluated Nuclear Data File (ENDF): <https://www-nds.iaea.org/exfor/endl.htm>.

7.1 Elastic collisions, friction force and the effect on the shock structure

The mean momentum exchanged along the flow direction in an elastic collision between a neutron of mass $A_n m_p$, with $A_n = 1.0013$, and an ion of mass $A_\alpha m_p$ is:

$$\langle \Delta p_{n\alpha} \rangle = - \frac{A_\alpha A_n}{A_\alpha + A_n} m_p \Delta \beta_{n\alpha} \cdot c, \quad (26)$$

Here we assumed for simplicity a point-like neutron scattered off a spherical ion with a uniform differential cross section ($\frac{d\sigma}{d\Omega} = \text{const}$). Taking $r_{\text{nucleon}} \sim 1.2 \text{ fm}$, the total cross-section is approximated by $\sigma_{n\alpha} = \pi r_{\text{nucleon}}^2 = \pi \cdot 1.2^2 \text{ fm}^2 \cdot A_\alpha^{2/3} = 4.5 \cdot 10^{-2} A_\alpha^{2/3} \sigma_T$.

The resultant force per unit volume acting on the neutron fluid by ion beam of type α is:

$$\mathcal{F}_{n\alpha} = n_n v_{n\alpha} \langle \Delta p_{n\alpha} \rangle, \quad (27)$$

where $v_{n\alpha}$ is the elastic scattering rate given by:

$$v_{n\alpha} = n_\alpha \sigma_{n\alpha} |\Delta \beta_{n\alpha} \cdot c|. \quad (28)$$

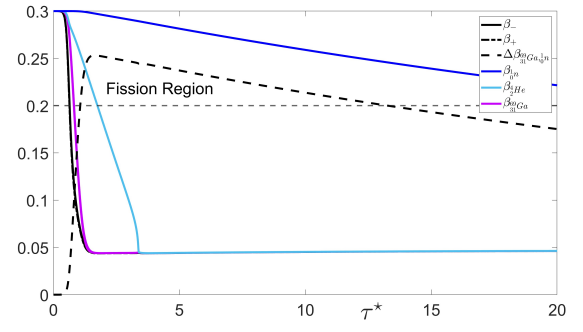
Momentum conservation readily implies $\mathcal{F}_{\alpha n} = -\mathcal{F}_{n\alpha}$. Since $\sum_\alpha \mathcal{F}_{n\alpha} = A_n m_p n_n \beta_n n_e \sigma_T \frac{d\beta_n}{d\tau} c^2$, one finds:

$$\begin{aligned} \frac{d\beta_n}{d\tau} &= -4.5 \cdot 10^{-2} \cdot \sum_\alpha \frac{1}{\beta_n} \frac{n_\alpha}{n_e} \frac{A_\alpha^{5/3}}{A_\alpha + A_n} |\Delta \beta_{n\alpha}| \Delta \beta_{n\alpha} \\ &= -4.5 \cdot 10^{-2} \cdot \sum_\alpha \frac{\beta_e}{\beta_n} \frac{\tilde{f}_\alpha}{\beta_\alpha} \frac{A_\alpha^{5/3}}{A_\alpha + A_n} |\Delta \beta_{n\alpha}| \Delta \beta_{n\alpha}. \end{aligned} \quad (29)$$

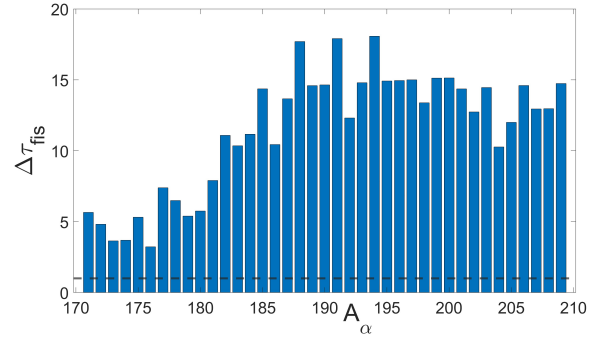
The force exerted on the ion fluid α by the neutrons can be added to Eq. (5.1), with the friction coefficient given by:

$$\tilde{g}_{\alpha n} \equiv 4.5 \cdot 10^{-2} \frac{A_n A_\alpha^{5/3}}{A_\alpha + A_n} |\Delta \beta_{n,\alpha}|. \quad (30)$$

Fig. 12 depicts the shock structure and neutron-heavy ions fission rates, including free neutrons, for the same parameters used in Fig. 8. We added free neutrons with $\tilde{f}_n = 1$ (corresponding to the pre-freeze-out region in the r-process case), which means we have about 10 neutrons per ion, giving significant fission rates. Reducing the neutrons fraction to ~ 1 neutron per ion ($\tilde{f}_n = 0.1$), for the same shock properties, will linearly reduce the fission rate to the critical value of 1. Note that at earlier times, density and temperature may be higher ($\theta \sim 0.2$ and $n_e \gtrsim 10^{27} \text{ cm}^{-3}$). This, however, does not alter the conclusions, showing similar results to fig. 12.



(a)



(b)

Figure 12. (a) Shock profile moving through r-process ambient with $69 \leq A \leq 209$, $n_e = 10^{25} \text{ cm}^{-3}$ and $\tilde{f}_n = 1$ at $\beta_u = 0.3$. Energies higher than the fission barrier are obtained within the mentioned region. All charged particles are coupled, where the ^{69}Ga red line represents their profile. (b) Number of collisions for heavy ions above the fission barrier region. Fission barriers, based on the finite-range liquid drop model (FRLDM), are taken from Möller et al. 2015. Cross-sections are taken to be geometrical.

7.2 Neutron-induced transmutation

We have seen that elastic collisions cannot couple the neutrons to the ions and the electrons. Hence, in the frame of the shock downstream, which has a sub-MeV temperature and a velocity of $(6/7)\beta_u$ compared to the upstream, the neutrons have a kinetic energy of about $0.4 \cdot m_p \beta_u^2 \approx 40 \beta_{u,0.3}^2 \text{ MeV}$. This exceeds the activation energy for most interactions. The effect of the sudden “heating” of the neutrons during times at which the nucleo-synthesis starts to fall out of equilibrium, but before freeze-out, is beyond the scope of this work. Yet we expect it to be significant.

8 APPLICATION TO BNS MERGERS

The nucleosynthesis of r-process elements in the outflow of BNS mergers takes place during the first second or so following its ejection, as the neutron-rich material decompresses. The exact evolution of the thermodynamic conditions as well as the nuclear reaction chain within each fluid element depends on its initial state and expansion velocity (e.g., Korobkin et al. 2012). As long as nuclear reactions (neutron capture, fission, etc.) take place, the temperature of the gas remains roughly 50 keV and the free neutrons are overabundant (dominate the number density). A sharp transition in the thermodynamic evolution takes place when the reactions terminate, roughly a second after the ejection at a density of about 100 gr cm^{-3} . In the first stage, almost all of the free neutrons are captured over a

very short time scale (much shorter than a second). Subsequently, the density and temperature evolve as in a freely expanding radiation-dominated gas, $\rho \propto t^{-3}$ and $T \propto t^{-1}$. The composition during this stage evolves only by radioactive decay towards the valley of stability. As we discuss below, this evolution implies that the properties of a shock that is driven into the ejecta strongly depend on whether it propagates in the ejecta before or after nuclear reactions freeze out.

Several different shocks are expected to cross the sub-relativistic material ejected from a BNS merger. First, in the commonly accepted scenario, and as supported by observations of GW170817, a jet is launched from the compact remnant formed in the aftermath of BNS coalescence and propagates through the merger ejecta. The motion of the jet inflates an expanding cocoon that drives an asymmetric RMS in the ejecta. The shock velocity is fastest along the jet axis (can approach the speed of light) and decreases with increasing angle. The angular distribution of the shock velocity depends on the density distribution of the ejecta, as well as the jet luminosity and opening angle, and is not known exactly. However, simulations suggest that it can exceed $0.1c$ and even approach $0.3c$ over a significant range of angles (Gottlieb & Nakar 2022). Overall, a small fraction (of an order of a few percent) of the ejecta is shocked by the jet and the cocoon. This material is expected to dominate the early KN emission, on time scales of minutes to hours (Gottlieb et al. 2018a; Hamidani & Ioka 2023, 2022). The shock can cross the ejecta both before or after the nucleosynthesis freeze-out and affect the composition of the cocoon material. A significant change in the composition of this material might affect the properties of the early kilonova signal.

A second source of shocks is the interaction between various components of the ejecta itself. There are several different mechanisms that expel matter, each operates on a different time scale after the merger and produces outflow with a different range of velocities (see, e.g., Nakar 2020 and references within). Since some of these produce relatively fast ejecta over long time scales, shocks are expected to form when different components of the outflow collide. For example, Nedora et al. (2021) find a fast ($0.15\text{--}0.3\text{ c}$) spiral-wave driven wind that lasts as long as the central remnant does not collapse to a black hole. This fast material, which may be ejected for a second or longer, is expected to interact with slower material, driving shocks at a velocity of $\sim 0.1\text{--}0.2\text{ c}$. Observations of GW170817 reveal a comparable amount of mass in ejecta having a velocity of $0.2\text{--}0.3\text{ c}$ and ejecta with a velocity of $0.1\text{--}0.2\text{ c}$. It is also likely that an even faster material was ejected. It is plausible that collisions during the ejection of this fast component generated shocks with velocities in the range $\sim 0.1\text{--}0.2\text{ c}$, and possibly even faster. These types of shocks form during the main mass ejection episode and, therefore, most likely cross the ejecta before the nucleosynthesis freeze-out, although it is conceivable that some shocks form also at later times.

Finally, the central remnant may also drive a quasi-spherical, or a wide-angle, shock into the ejecta. For example, a long-lasting magnetar can inject enough energy to significantly accelerate the ejected material, thereby driving a fast shock through a large fraction of the ejecta (e.g., Beloborodov et al. 2020). This may even be the source of the fast ($\sim 0.3\text{ c}$) component in GW170817. Such energy injection can ensue before and/or after the nucleosynthesis freeze-out and may have a significant effect on the composition of most of the ejecta

8.1 Alpha particles

Estimates based on the observed kilonova emission in GW170817 indicate ejecta mass of $M_{ej} \approx 10^{-2} M_{\odot}$. The corresponding density

at a radius $r = 10^{10} r_{10}\text{ cm}$ is $\rho \approx 10(M_{ej}/10^{-2} M_{\odot}) r_{10}^{-3}\text{ gr cm}^{-3}$. The blackbody temperature in the far downstream, achieved when the downstream plasma reaches full thermodynamic equilibrium, is $kT_{d,BB} = 60(\rho/10\text{ gr cm}^{-3})^{1/4}(\beta_u/0.3)^{1/2}\text{ keV}$. This is a strict lower limit on the temperature just behind the shock. In case of r-process rich upstream, Levinson & Nakar (2020) find that for a single-fluid RMS model, if no pairs are created, the immediate downstream falls out of equilibrium at $\beta_u > 0.25(\rho/10\text{ gr cm}^{-3})^{1/30}$, whereupon the temperature inside and just behind the shock is significantly higher than $kT_{d,BB}$. We therefore conclude that for shocks with $\beta_u > 0.25$ that cross the ejecta within the first few seconds the downstream temperature is expected to exceed 50 keV , leading to excessive pair creation and, consequently, a large abundance of positrons inside the shock (Katz et al. 2010; Budnik et al. 2010; Levinson & Nakar 2020). According to the results obtained in 6, such overabundance of positrons will lead to both, a reduction in the physical shock width and nearly complete screening of the electrostatic field inside the shock. As a result, binary Coulomb collisions of pairs and ions, which under such conditions becomes the dominant coupling mechanism, is not strong enough to prevent decoupling of the alpha particles from the heavy ions cluster within the shock transition layer. Then, collisions between neutron-rich isotopes and alpha particles just behind the shock may be strong enough to trigger fission and fusion. This can lead to a substantial composition change, provided anomalous friction does not prevent full decoupling inside the shock. Below, we provide an estimate of the scale separation (between radiation and kinetic scales) and discuss the implications of anomalous coupling.

8.2 Free neutrons

As mentioned above, a large abundance of free neutrons is present in the ejecta up to about one second post-merger. If the shock propagates in the ejecta during this stage, free neutrons advected with the upstream flow will cross the shock undisturbed and collide with the heavy nuclei downstream. This can trigger fission, provided that the relative velocity of the free neutrons with respect to the downstream ions exceeds the fission barrier. Fission barriers of heavy ions, at or near the valley of stability, range from a few MeV for atomic numbers $Z > 80$ roughly (depending on A), to about 40 MeV for lighter elements (Möller et al. 2009; Royer et al. 2021). For most ions with $Z > 70$ it is roughly 20 MeV . According to the results in 7, the energy of free neutrons in the downstream exceeds this value at shock velocities $\beta_u \gtrsim 0.25$. Prior to freeze-out, all the nuclei are far from the valley of stability and, therefore, even lower energy neutrons are likely to cause transmutations of heavy nuclei. Finding the effect of the sudden heating of free neutrons by shocks, after nucleosynthesis starts to fall out of equilibrium and before freeze-out, on the final ejecta composition is out of the scope of this paper. Yet, we suspect it to be significant.

8.3 Scale separation and coupling length

In section 5, we demonstrated that sufficiently strong collective inter-ionic friction can tightly couple the ions, preventing relative drifts, when binary collisions fail to do so. As explained there, in reality, such friction represents anomalous momentum transfer between ions via scattering off plasma turbulence. Such momentum transfer occurs on microscopic scales, but the actual length scale is unclear at present. In Vanthieghem et al. (2022) it has been shown, by means of PIC simulations, that in a single-ion RRMS,

where positrons are present, the anomalous coupling length scales as $l_c \sim 10^5 M^{1/2} (\gamma_u/10)^{-1} l_p$, where M is the pair multiplicity, γ_u the shock Lorentz factor and l_p the proton skin depth defined below. For the typical densities expected in many exploding stellar systems (e.g., SNe, LGRB) l_c has been shown to be much smaller than the shock width (by several orders of magnitude). This result is probably irrelevant to the Newtonian, multi-ion RMS studied here, as the plasma modes that dominate the turbulence are most likely different. However, it suggests that the anomalous coupling length may encompass thousands or even tens of thousands of skin depths. At the extreme densities of BNS merger ejecta, this may exceed the shock width, as we now show.

To get a rough measure of the anticipated scale separation in RMS, we compare the Thomson length, $l_T = (\sigma_T n_{e,u})^{-1}$, with the proton skin depth at the same density, $l_p = c/\omega_p = (m_p c^2 / 4\pi e^2 n_{e,u})^{1/2}$ ¹. The upstream electron number density can be estimated upon assuming that all elements have $Z/A = 0.5$:

$$n_{e,u} \approx \frac{\rho}{2m_p} \approx 10^{25} (M_{ej}/10^{-2} M_\odot) r_{10}^{-3} \text{ cm}^{-3}, \quad (31)$$

from which we find

$$l_T/l_p \approx 10^4 \left(\frac{n_{e,u}}{10^{25} \text{ cm}^{-3}} \right)^{-1/2}. \quad (32)$$

Note that this ratio scales as $r_{10}^{3/2}$. Comparing the ratio l_T/l_c in the last equation with the ion collision depth in Fig. 8 suggests that if indeed $l_c > 10^4 l_p$, anomalous coupling may not prevent inelastic ion-ion collisions, and the consequent change of the composition profile. A more firm conclusion requires a quantitative analysis of plasma instabilities in the multi-ion system, which is beyond the scope of this paper. We defer such analysis for a future study.

9 SUMMARY

We have demonstrated how the passage of a fast radiation-mediated shock through a multi-ion plasma can lead to significant drift velocities between various plasma constituents. The reason is that ions having different charge-to-mass ratios experience different deceleration rates by the electrostatic field generated inside the shock, owing to the charge separation imposed by the radiation force acting solely on the electrons. We have also shown that the presence of pairs and/or free neutrons enhance the expected drift velocities, while anomalous friction due to plasma instabilities is acting to reduce the drift velocities.

Drift velocities will, first, lead to the generation of micro-turbulence which can in turn lead to the acceleration of particles, thereby affecting the emission from such shocks upon breakout, as well as other properties of the shock. Most interestingly, for shocks that are fast enough the development of significant drift velocities can trigger nuclear reactions in the immediate shock downstream, thereby changing the composition behind the shock.

In case of BNS mergers, we find that nuclear reactions might be triggered by shocks that cross the ejecta during the first few seconds after the merger at velocities $\beta_u \gtrsim 0.25$. If the shocks cross the ejecta before nucleosynthesis freeze-out in the unshocked ejecta (roughly 1 s after merger), the highly abundant free neutrons are heated to temperatures of tens of MeV (compared to sub-MeV temperatures

before shock crossing). This process is not affected by anomalous friction. While we do not compute the effect of such heating on the final composition, we expect it to be significant. If fast shocks cross the ejecta after nucleosynthesis freeze-out, collisions of α particles with heavy ions in the immediate downstream are expected, possibly leading to nuclear transmutation. We have shown that the separation between radiation and kinetic scales in merger ejecta is small enough to possibly prevent anomalous friction from playing a significant role in these systems. The resultant change in composition behind the shock that the jet drives as it crosses the ejecta, might considerably affect the properties of the early kilonova emission (minutes to hours), which is likely dominated by the cocoon. The late kilonova emission can be also affected if fast shocks arise between different components of the ejecta or if the central remnant injects a significant amount of energy into the outflow after its ejection.

In SNe, if significant drift velocities are not prevented by anomalous friction, proton capture reactions are found to be important at shock velocity $\beta_u \gtrsim 0.2$, even if the abundance of H is smaller than solar by several orders of magnitudes. Such high velocities are not expected in type II SNe, but are likely in type Ib/c SNe and in shock breakout from extended stellar envelopes in IIGRB (Nakar 2015). The absence of hydrogen lines in the spectra of these SNe sets a limit on the H abundance; according to Hachinger et al. (2012) an H mass fraction of even 1% out of the total may be allowed, where the H mass fraction in the outer envelope can be considerably higher. What would be the effect of the composition change on the emitted spectrum in these sources is unclear at present, although it would probably affect only spectra at very early times. We hope that future studies might be able to identify observational diagnostics that can test this model.

Our analysis ignores the effect of anomalous friction due to plasma instabilities. An estimate of the ratio between kinetic and radiation scales is given in Sec. 8.3. Based on this estimate, we speculated that in BNS mergers, owing to the extreme density of the ejecta, anomalous coupling may not prevent a complete velocity separation between He and the heavy ions, hence, may not affect our results significantly. In SNe, where the typical densities are smaller by about ten orders of magnitudes, the scale separation is much larger and the effect of beam instabilities on the downstream velocity distribution of the ions is unclear. We point out that if the threshold drift velocity required for anomalous coupling is large enough, it may lead to formation of collisionless subshocks, with random ion velocities in excess of the proton capture barrier. Otherwise, the onset of instabilities might suppress nuclear reactions in SNe. We plan to conduct a detailed kinetic study of instabilities in multi-ion RMS, along similar lines to the study described in Vanthieghem et al. (2022), in the near future.

DATA AVAILABILITY

The data underlying this article will be shared on reasonable request to the corresponding author.

ACKNOWLEDGEMENTS

We thank Israel Mardor and Heinrich Wilsenach for enlightening discussions on nuclear physics. This research was partially supported by an Israel Science Foundation grant 1995/21 and a consolidator ERC grant 818899 (JetNS).

¹ The skin depth of an individual ion beam α is related to the proton skin depth through: $l_\alpha = \sqrt{n_{e,u} A_\alpha / n_{\alpha,u} Z_\alpha^2} l_p \simeq l_p$.

REFERENCES

- Bass R., 1973, *Phys. Lett. B*, 47, 139
- Beloborodov A. M., Lundman C., Levin Y., 2020, *ApJ*, 897, 141
- Blandford R. D., Payne D. G., 1981a, *MNRAS*, 194, 1033
- Blandford R. D., Payne D. G., 1981b, *MNRAS*, 194, 1041
- Budnik R., Katz B., Sagiv A., Waxman E., 2010, *Astrophys. J.*, 725, 63
- Chevalier R. A., Soderberg A. M., 2010, *The Astrophysical Journal Letters*, 711, L40
- Derishev E., 2018, *Astronomy Reports*, 62, 868
- Gilkis A., Arcavi I., 2022, *MNRAS*, 511, 691
- Goriely S., 1999, *A&A*, 342, 881
- Gottlieb O., Nakar E., 2022, *MNRAS*, 517, 1640
- Gottlieb O., Nakar E., Piran T., 2018a, *MNRAS*, 473, 576
- Gottlieb O., Nakar E., Piran T., Hotokezaka K., 2018b, *MNRAS*, 479, 588
- Hachinger S., Mazzali P. A., Taubenberger S., Hillebrandt W., Nomoto K., Sauer D. N., 2012, *MNRAS*, 422, 70
- Hamidani H., Ioka K., 2022, *arXiv e-prints*, p. arXiv:2210.02255
- Hamidani H., Ioka K., 2023, *MNRAS*, 520, 1111
- Ito H., Levinson A., Nakar E., 2020, *Monthly Notices of the Royal Astronomical Society*, 499, 4961
- Kasliwal M. M., et al., 2017, *Science*, 358, 1559
- Katz B., Budnik R., Waxman E., 2010, *Astrophys. J.*, 716, 781
- Korobkin O., Rosswog S., Arcones A., Winteler C., 2012, *MNRAS*, 426, 1940
- Kox S., et al., 1987, *Phys. Rev. C*, 35, 1678
- Levinson A., 2020, *Phys. Rev. E*, 102
- Levinson A., Nakar E., 2020, *Phys. Rep.*, 866, 1
- Levinson A., Granot A., Vanthieghem A., Mahlmann J., 2023, *Journal of Plasma Physics*, 89, 915890301
- Lippuner J., Roberts L. F., 2017, *ApJS*, 233, 18
- Lodders K., 2019, *arXiv e-prints*, p. arXiv:1912.00844
- Mahlmann J. F., Vanthieghem A., Philippov A. A., Levinson A., Nakar E., Fiuza F., 2023, *MNRAS*, 519, 6126
- Margutti R., Chornock R., 2021, *ARA&A*, 59, 155
- Möller P., Sierk A. J., Ichikawa T., Iwamoto A., Bengtsson R., Uhrenholt H., Åberg S., 2009, *Phys. Rev. C*, 79, 064304
- Möller P., Sierk A. J., Ichikawa T., Iwamoto A., Mumpower M., 2015, *Phys. Rev. C*, 91, 024310
- Mooley K. P., et al., 2018, *Nature*, 561, 355
- Nakar E., 2015, *ApJ*, 807, 172
- Nakar E., 2020, *Phys. Rep.*, 886, 1
- Nakar E., Gottlieb O., Piran T., Kasliwal M. M., Hallinan G., 2018, *ApJ*, 867, 18
- Nedora V., et al., 2021, *ApJ*, 906, 98
- Royer G., Guillot M., Monard J., 2021, *Nuclear Phys. A*, 1010, 122191
- Soppera N., Dupont E., Bossant M., 2012, *JANIS Book of proton-induced cross-sections* (2012)
- Tarumi Y., Hotokezaka K., Domoto N., Tanaka M., 2023, *arXiv e-prints*, p. arXiv:2302.13061
- Vanthieghem A., Mahlmann J. F., Levinson A., Philippov A., Nakar E., Fiuza F., 2022, *MNRAS*, 511, 3034
- Waxman E., Katz B., 2017, *Shock Breakout Theory*, p. 967
- Weaver T. A., 1976, *Astrophysical Journal Supplement Series*, vol. 32, Oct. 1976, p. 233-282., 32, 233

APPENDIX A: DERIVATION OF SHOCK EQUATIONS

We consider a planar shock propagating in the $-\hat{x}$ direction through a static, fully ionized, infinite cold medium. In the shock frame the flow is steady, with an upstream velocity $\beta_u \lesssim 0.5$ in the \hat{x} direction. We suppose that the plasma upstream of the shock is made of electrons and various ion species (henceforth labeled by a subscript α) of atomic number Z_α and mass number A_α . We further assume that the energy dissipated inside the shock is fully converted into radiation, which is a good approximation in RMS. For simplicity, we

neglect pair production inside the shock (which may not be justified at extreme densities, see Sec. 8 for details) and any other conversion process (e.g., nuclear transmutations). In the multi-fluid approach developed here, the electrons and the different ion species are treated as different fluid components, with densities n_e and n_α , respectively, and velocities β_e and β_α . Since we neglect conversion processes, all particle fluxes must be conserved across the shock, viz., $j_e \equiv n_e \beta_e = \text{const}$, and likewise for $j_\alpha \equiv n_\alpha \beta_\alpha$.

Following Blandford & Payne (1981a), we invoke the diffusion approximation to compute the transfer of radiation through the shock. Since, practically, only the electrons experience the radiation force (through inverse Compton scattering), the advection velocity must equal β_e . The energy flux of the radiation (in units of $c = \hbar = 1$) can then be expressed as (Blandford & Payne 1981a; Levinson & Nakar 2020):

$$T_\gamma^{0x} = \beta_e(e_\gamma + p_\gamma) - \frac{1}{3n_e\sigma_T} \partial_x e_\gamma, \quad (\text{A1})$$

where e_γ and p_γ are the radiation energy density and pressure, respectively. The first term on the R.H.S describes the advection of enthalpy, and the second term the diffusion flux (Fick's law), with the diffusion coefficient averaged over all angles (hence the $1/3$ factor). Treating the radiation as a relativistic gas, we can use the equation of state $e_\gamma = 3p_\gamma$ to close the system of moment equations. With the normalization $\pi_\gamma = p_\gamma/m_e j_e$ and $\tilde{T}_\gamma^{0x} = T_\gamma^{0x}/m_e j_e$, Eq. (A1) reads:

$$\tilde{T}_\gamma^{0x} = 4\pi_\gamma \beta_e - \partial_\tau \pi_\gamma. \quad (\text{A2})$$

Under the assumption that the plasma is cold, the energy fluxes of the electron and ion fluids are given by $T_e^{0x} = \frac{1}{2}m_e n_e \beta_e^3$ and $T_\alpha^{0x} = \frac{1}{2}A_\alpha m_p n_\alpha \beta_\alpha^3$, respectively. In terms of the Thomson optical depth, $d\tau = n_e \sigma_T dx$, energy conservation across the shock can be expressed as,

$$\partial_\tau (T_\gamma^{0x} + T_e^{0x} + \sum_\alpha T_\alpha^{0x}) = 0. \quad (\text{A3})$$

To the order we are working in, the momentum fluxes of the radiation and the electron fluid are, respectively, $T_\gamma^{xx} = p_\gamma$ and $T_e^{xx} = m_e n_e \beta_e^2 = m_e j_e \beta_e$. The change in the momentum flux of the coupled electron-photon system must equal the electrostatic force density acting on the electrons:

$$\partial_x (T_e^{xx} + T_\gamma^{xx}) = -en_e E. \quad (\text{A4})$$

Dividing by $m_e j_e$ and using our normalization, we obtain Eq. (5),

$$\partial_\tau (\pi_\gamma + \beta_e) = -\tilde{E}. \quad (\text{A5})$$

Likewise, the momentum flux of ion species α is $T_\alpha^{xx} = m_p A_\alpha n_\alpha \beta_\alpha^2 = m_p A_\alpha j_\alpha \beta_\alpha$. The change in this momentum flux must equal the electrostatic force density acting on the ions:

$$\partial_x T_\alpha^{xx} = eZ_\alpha n_\alpha E. \quad (\text{A6})$$

Dividing by $m_p A_\alpha j_\alpha$ and normalizing we obtain Eq. (6). To obtain Eq. (7) we note that $\partial_x T_\alpha^{0x} = \beta_\alpha \partial_x T_\alpha^{xx} = eZ_\alpha j_\alpha E$. Likewise, $\partial_x T_e^{0x} = \beta_e \partial_x T_e^{xx} = -e j_e E - \beta_e \partial_x T_\gamma^{xx}$, where Eq. (A4) has been employed.

By summing over all ions and using Eq. (1), we find

$$\partial_x (T_e^{0x} + \sum_\alpha T_\alpha^{0x}) = -\beta_e \partial_x T_\gamma^{xx} = -\beta_e \partial_x p_\gamma. \quad (\text{A7})$$

Combining the last equation with Eqs. (A2)-(A3), we finally arrive at Eq. (7):

$$\partial_\tau \tilde{T}_\gamma^{0x} = \partial_\tau (4\pi_\gamma \beta_e - \partial_\tau \pi_\gamma) = \beta_e \partial_\tau \pi_\gamma. \quad (\text{A8})$$

A1 Inclusion of interspecies friction

We suppose that the change in momentum of species a ($a = e$ for electrons and $a = \alpha$ for ions) due to momentum exchange with species a' is proportional to the relative velocity between the two beams and the density of the a' beam: $\mathcal{F}_{aa'} = g_{aa'} n_{a'} (\beta_a - \beta_{a'})$, where $g_{aa'}$ is a characteristic friction coefficient that, in general, can depend on the velocities and temperatures of the colliding fluids. With friction forces included, the momentum equations of the electrons and ions read:

$$\partial_x (T_e^{xx} + T_\gamma^{xx}) = -en_e E + \sum_\alpha n_e \mathcal{F}_{e\alpha}, \quad (\text{A9})$$

$$\partial_x T_\alpha^{xx} = eZ_\alpha n_\alpha E + \sum_{\alpha'} n_\alpha \mathcal{F}_{\alpha\alpha'} + n_\alpha \mathcal{F}_{\alpha e}. \quad (\text{A10})$$

The anti-symmetry of the interspecies forces, $n_a \mathcal{F}_{aa'} + n_{a'} \mathcal{F}_{a'a} = 0$, guarantees momentum conservation of the entire system (plasma and radiation). However, since friction forces are dissipative (non-conservative), additional physics is needed to specify how the dissipation energy is distributed. Here, we adopt a simplified treatment that invokes ad hoc energy transfer between ions and electrons over length scales much shorter than the radiation length. Specifically, we assume that the electron and ions fluids remain highly super-sonic at all times. Under this assumption the energy fluxes of the electrons and ions can still be expressed as $T_e^{0x} = \frac{1}{2} m_e n_e \beta_e^3$ and $T_\alpha^{0x} = \frac{1}{2} A_\alpha m_p n_\alpha \beta_\alpha^3$, respectively, whereby $\partial_x T_a^{0x} = \beta_a \partial_x T_a^{xx}$ for $a \in [e, \alpha]$. Energy conservation, Eq. (A3), then yields

$$\partial_x \tilde{T}_\gamma^{0x} = - \sum_a \beta_a \partial_x \tilde{T}_a^{xx} = \beta_e \partial_x p_\gamma - \sum_{a,a'} n_a \beta_a \mathcal{F}_{aa'}, \quad a \in [e, \alpha]. \quad (\text{A11})$$

A2 Inclusion of positrons

We now re-derive the equations assuming that a fixed number of positrons is contained the upstream flow. We denote the density of positrons by n_+ and the total density of electron by n_e as before. The corresponding conserved fluxes are $j_+ = n_+ \beta_+$ and $j_e = n_e \beta_e$. The pair multiplicity is defined as $M = n_{+,u} / (n_{e,u} - n_{+,u})$, noting that $n_e - n_+ = \sum_\alpha n_\alpha Z_\alpha$ is the total number of protons in the system. The neutrality condition now reads:

$$\sum_\alpha j_\alpha Z_\alpha + j_+ = j_e. \quad (\text{A12})$$

We normalize all quantities as before in terms of the total electron flux n_e and flux j_e . The optical is then $d\tau = \sigma_T n_e dx$, and the fiducial electric field E_0 , the parameter χ and the radiation pressure are expressed as before in terms of j_e . With positrons included, Gauss' equation, Eq. (3), becomes

$$\partial_\tau \tilde{E} = \chi \left[-1 + \frac{M\beta_-}{(1+M)\beta_+} + \sum \frac{\beta_- j_\alpha Z_\alpha}{\beta_\alpha j_e} \right]. \quad (\text{A13})$$

Since the radiation is coupled to positrons in addition to electrons, the advection of radiation in the shock depends on both β_e and β_+ , and Eq. (A1) is no longer valid. We settle for a simple prescription, defining

$$\tilde{T}_\gamma^{0x} = 4\pi\gamma \left(\frac{n_e \beta_e}{n_e + n_+} + \frac{n_+ \beta_+}{n_e + n_+} \right) - \frac{n_e}{n_e + n_+} \partial_\tau \pi_\gamma. \quad (\text{A14})$$

The momentum flux of the radiation remains $T_\gamma^{xx} = p_\gamma$. Now, the momentum transferred to the electron fluid by the radiation at any given position is proportional to the relative number of scatterings,

$n_e / (n_e + n_+)$, and likewise for the positron fluid. Consequently, the momentum equations for the electron and positron fluids are, respectively,

$$\begin{aligned} \partial_x \left(T_e^{xx} + \frac{n_e}{n_e + n_+} p_\gamma \right) &= -en_e E + n_e \mathcal{F}_{e+} + \sum_\alpha n_e \mathcal{F}_{e\alpha}, \\ \partial_x \left(T_+^{xx} + \frac{n_+}{n_e + n_+} p_\gamma \right) &= en_+ E + n_+ \mathcal{F}_{+e} + \sum_\alpha n_+ \mathcal{F}_{+\alpha}. \end{aligned} \quad (\text{A15})$$

The ion momentum equation reads:

$$\partial_x T_\alpha^{xx} = eZ_\alpha n_\alpha E + \sum_{\alpha'} n_\alpha \mathcal{F}_{\alpha\alpha'} + n_\alpha \mathcal{F}_{\alpha e} + n_\alpha \mathcal{F}_{\alpha+}. \quad (\text{A16})$$

It is readily seen that the sum gives

$$\partial_x \left(T_e^{xx} + T_+^{xx} + \sum_\alpha T_\alpha^{xx} + p_\gamma \right) = 0, \quad (\text{A17})$$

as required from momentum conservation.

From energy conservation, $\partial_\tau (T_\gamma^{0x} + T_e^{0x} + T_+^{0x} + \sum_\alpha T_\alpha^{0x}) = 0$, and the neutrality condition, Eq. (A12), we finally arrive at

$$\partial_x T_\gamma^{0x} = \beta_e \partial_x \left(\frac{n_e}{n_e + n_+} p_\gamma \right) + \beta_+ \partial_x \left(\frac{n_+}{n_e + n_+} p_\gamma \right) - \sum_{a,a'} n_a \beta_a \mathcal{F}_{aa'}, \quad (\text{A18})$$

here $a \in [e, +, \alpha]$. Note that if the pairs are strongly coupled, $\beta_e = \beta_+$, the sum of the first two terms on the R.H.S. reduces to $\beta_e \partial_x p_\gamma$, as expected.

APPENDIX B: DERIVATION OF COULOMB FRICTION COEFFICIENTS

We consider a gas of particles of type a with bulk velocity $\beta_a c$ and number density n_a moving into a gas of a' particles. a and a' can either be an ion isotope ($\frac{A}{Z}\alpha$) or electrons (with subscript e , taking the values $Z_e = -1$ and $A_e = \mu \equiv \frac{m_e}{m_p}$). The general force per unit volume acting on the gas of type a moving through a gas of a' particles is:

$$\mathcal{F}_{aa'} = -m_a n_a v_{aa'} \Delta v_{\text{drift}, aa'}. \quad (\text{B1})$$

Where $v_{aa'}$ is the coulomb interaction rate given by:

$$v_{aa'} = \sqrt{2\pi} \frac{4}{3} n_{a'} \frac{Z_a^2 Z_{a'}^2 e^4 (A_a + A_{a'})}{A_a^2 A_{a'} m_p^2 \Delta \beta_{aa'}^3 c^3} \ln \Lambda_{aa'}. \quad (\text{B2})$$

The logarithmic factor $\Lambda_{aa'}$ comes out of integrating between minimal and maximal impact parameters. We used $r_{\min} = \max \left\{ \frac{4\pi Z_a Z_{a'} e^2}{A_a A_{a'} \Delta \beta_{aa'}^2 m_p c^2} (A_a + A_{a'}), \frac{\hbar c}{A_a A_{a'} \Delta \beta_{aa'} m_p c} (A_a + A_{a'}) \right\}$ and $r_{\max} = \lambda_{\text{debye}} = \sqrt{\frac{\theta_e m_e c^2}{4\pi n_e e^2}}$. All together one finds:

$$\begin{aligned} \Lambda_{aa'} &= \frac{r_{\max}}{r_{\min}} = \\ &= \frac{1}{\mu (4\pi)^{3/2}} \cdot \frac{(m_e c^2)^{3/2}}{(e^2)^{3/2}} \cdot \frac{A_a A_{a'}}{Z_a Z_{a'} (A_a + A_{a'})} \cdot \frac{\theta_e^{1/2}}{n_e^{1/2}} \Delta \beta_{aa'}^2 = \\ &= 2.6 \cdot 10^{20} \cdot \frac{A_a A_{a'}}{Z_a Z_{a'} (A_a + A_{a'})} \cdot \frac{\theta_e^{1/2}}{n_e^{1/2}} \Delta \beta_{aa'}^2. \end{aligned} \quad (\text{B3})$$

In case $r_{\min} > r_{\max}$ the interaction is totally screened and we set

$\Lambda_{aa'} \equiv 1$ so that $\log \Lambda_{aa'} = 0$. Regarding $\Delta\beta_{aa'}^2$, one has to take into account both the relative drift and thermal velocity. We obtain:

$$\begin{aligned} \Delta\beta_{aa'}^2 &= \Delta\beta_{drift,aa'}^2 + \Delta\beta_{thermal,aa'}^2 = \\ &= (\beta_a - \beta_{a'})^2 + 2\mu \left(\frac{\theta_a}{A_a} + \frac{\theta_{a'}}{A_{a'}} \right). \end{aligned} \quad (\text{B4})$$

Writing down the force equation in the shock parameters, $\mathcal{F}_{aa'} = A_a m_p n_a \beta_a n_e \sigma_T \frac{d\beta_a}{d\tau} c^2$, combining B1, one finds:

$$\frac{d\beta_a}{d\tau} = - \frac{\beta_e}{\beta_a A_a} \frac{\tilde{j}_{a'}}{\beta_{a'}} \frac{\mu^2}{\sqrt{2\pi}} \frac{A_a + A_{a'}}{A_a A_{a'}} Z_a^2 Z_{a'}^2 \frac{\ln \Lambda_{aa'}}{\Delta\beta_{aa'}^3} \Delta\beta_{drift,aa'} \quad (\text{B5})$$

where we used $\sigma_T = \frac{8\pi}{3} \cdot \frac{e^4}{m_e^2 c^4}$, $\mu \equiv \frac{m_e}{m_p}$, $\tilde{j}_{a'} \equiv \frac{n_{a'} \beta_{a'}}{n_e \beta_e}$ and $d\tau \equiv n_e \sigma_T dx$. Using previous notations we find:

$$\tilde{g}_{aa'} = \frac{\mu^2}{\sqrt{2\pi}} \frac{A_a + A_{a'}}{A_a A_{a'}} Z_a^2 Z_{a'}^2 \frac{\ln \Lambda_{aa'}}{\Delta\beta_{aa'}^3}. \quad (\text{B6})$$

To estimate the conditions under which relative drift would rise between the particles, we need to find when the thermal-dominated coupling breaks down. In case the interaction is temperature-dominated, assuming all particles own the same temperature $\theta_a = \theta_{a'} \equiv \theta$, one obtains $\Delta\beta_{aa'}^2 \approx 2\mu \theta \frac{A_a + A_{a'}}{A_a A_{a'}}$. This gives:

$$\tilde{g}_{aa'} = \sqrt{\frac{\mu}{16\pi} \cdot \frac{A_a A_{a'}}{A_a + A_{a'}}} Z_a^2 Z_{a'}^2 \frac{\ln \Lambda_{aa'}}{\theta^{3/2}} \quad (\text{B7})$$

with $\Lambda_{aa'} = 5.2 \cdot 10^{20} \frac{\mu}{Z_a Z_{a'}} \frac{\theta^{3/2}}{n_e^{1/2}}$.

Requiring complete ion-ion coupling is done by taking $\Delta\beta_{drift,aa'} = d\beta_a$ in B5. This enables us to find a relation between the length scale for inter-ionic coulomb friction coupling and the shock width $l_{sh} \equiv (\beta_u n_e \sigma_T)^{-1}$:

$$\begin{aligned} l_{aa'} &= \sqrt{\frac{16\pi}{\mu} \frac{A_a + A_{a'}}{A_a A_{a'}}} \beta_u^2 A_a \frac{n_e}{n_{a'}} \frac{\theta^{3/2}}{Z_a^2 Z_{a'}^2 \ln \Lambda_{aa'}} l_{sh} \\ &\approx 3 \cdot 10^2 \beta_u^2 \sqrt{\frac{A_a + A_{a'}}{A_a A_{a'}}} \frac{A_a}{Z_a} \frac{n_e}{Z_{a'} n_{a'}} \frac{\theta^{3/2}}{Z_a Z_{a'} \ln \Lambda_{aa'}} l_{sh}, \end{aligned} \quad (\text{B8})$$

where we assume $\Delta\beta_{aa'}^2 \propto \theta$, implying that this equation is valid as long as the thermal velocity is larger than the drift velocity. When $l_{aa'}$ exceeds l_{sh} , the different constituents can no longer be coupled within the shock, and relative drift arises. Taking $a = \alpha$ and $a' = e$, B8 reduces to

$$l_{\alpha e} = 1.3 \cdot 10^4 \frac{\theta_e^{3/2}}{\ln \Lambda_{\alpha e}} \frac{\beta_u^2 A_\alpha}{Z_\alpha^2} l_{sh}. \quad (\text{B9})$$

This paper has been typeset from a \LaTeX file prepared by the author.